

Extreme heterogeneity of influenza virus infection in single cells

Alistair B. Russell¹, Cole Trapnell², Jesse D. Bloom^{1,2*}

*For correspondence:
jbloom@fredhutch.org

¹Basic Sciences Division and Computational Biology Program, Fred Hutchinson Cancer Research Center, Seattle, United States; ²Department of Genome Sciences, University of Washington, Seattle, United States

Abstract Viral infection can dramatically alter a cell's transcriptome. However, these changes have mostly been studied by bulk measurements on many cells. Here we use single-cell mRNA sequencing to examine the transcriptional consequences of influenza virus infection. We find extremely wide cell-to-cell variation in production of viral gene transcripts – viral transcripts compose less than a percent of total mRNA in many infected cells, but a few cells derive over half their mRNA from virus. Some infected cells fail to express at least one viral gene, and this gene absence partially explains variation in viral transcriptional load. Despite variation in total viral load, the relative abundances of viral mRNAs are fairly consistent across infected cells. Activation of innate immune pathways is rare, but some cellular genes co-vary in abundance with the amount of viral mRNA. Overall, our results highlight the complexity of viral infection at the level of single cells.

Introduction

Viruses can cause massive and rapid changes in a cell's transcriptome as they churn out viral mRNAs and hijack cellular machinery. For instance, cells infected with influenza virus at high multiplicity of infection (MOI) express an average of 50,000 to 100,000 viral mRNAs per cell, corresponding to 5 to 25% of all cellular mRNA (Hatada *et al.*, 1989). Infection can also trigger innate-immune sensors that induce the expression of cellular anti-viral genes (Killip *et al.*, 2015; Iwasaki and Pillai, 2014; Crotta *et al.*, 2013). This anti-viral response is another prominent transcriptional signature of high-MOI influenza virus infection in bulk cells (Geiss *et al.*, 2002).

However, initiation of an actual influenza infection typically involves just a few virions infecting a few cells (Varble *et al.*, 2014; Poon *et al.*, 2016; Leonard *et al.*, 2017; McCrone *et al.*, 2017). The dynamics of viral infection in these individual cells may not mirror bulk measurements made on many cells infected at high MOI. Over 70 years ago, Max Delbrück showed that there was a ~100-fold range in the number of progeny virions produced per cell by clonal bacteria infected with clonal bacteriophage (Delbrück, 1945). Subsequent work has shown similar heterogeneity during infection with other viruses (Zhu *et al.*, 2009; Schulte and Andino, 2014; Combe *et al.*, 2015; Akpinar *et al.*, 2016), including influenza virus (Heldt *et al.*, 2015).

In the case of influenza virus infection, targeted measurements of specific proteins or RNAs have shed light on some factors that contribute to cell-to-cell heterogeneity. The influenza virus genome consists of eight negative-sense RNA segments, and many infected cells fail to express one more of these RNAs (Heldt *et al.*, 2015; Dou *et al.*, 2017) or their encoded proteins (Brooke *et al.*, 2013). In addition, activation of innate-immune responses is inherently stochastic (Shalek *et al.*, 2013, 2014; Bhushal *et al.*, 2017; Hagai *et al.*, 2017), and only some influenza-infected cells express anti-viral interferon genes (Perez-Cidoncha *et al.*, 2014; Killip *et al.*, 2017). However, the extent of cell-to-cell variation in these and other host and viral factors remains unclear, as does the

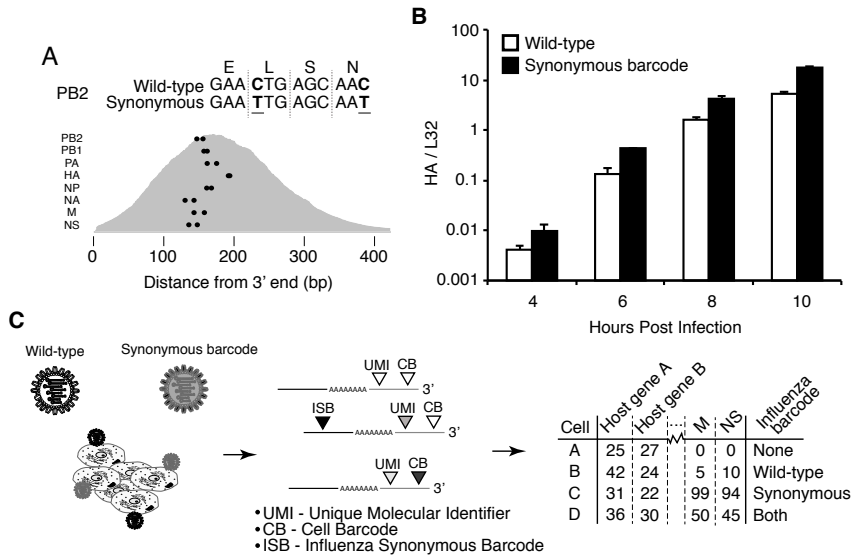


Figure 1. Experimental design. **(A)** We engineered a virus that carried two synonymous mutations near the 3' end of each mRNA. At top are the mutations for PB2. At bottom are locations of the synonymous mutations relative to the typical distribution of read depth for our 3'-end sequencing. **(B)** The wild-type and synonymously barcoded viruses transcribe their genes with similar kinetics. The abundance of the viral hemagglutinin (HA) transcript relative to the cellular housekeeping gene L32 was assessed by qPCR in A549 cells infected at an MOI of 0.5 (as determined on MDCK-SIAT1 cells). Error bars \pm S.D., n=3. **(C)** For the single-cell mRNA sequencing, A549 cells were infected with an equal mixture of wild-type and synonymously barcoded virus. Immediately prior to collection, cells were physically separated into droplets and cDNA libraries were generated containing the indicated barcodes. The libraries were deep sequenced, and the data processed to create a matrix that gives the number of molecules of each transcript observed in each cell. Infected cells were further annotated by whether their viral mRNAs derived from wild-type virus, synonymously barcoded virus, or both.

Figure 1-source data 1. Sequences of wild-type and barcoded viruses are in [viralsequences.fasta](#).

43 association among them in individual infected cells.

44 Here we use single-cell mRNA sequencing to quantify the levels of all cellular and viral mRNAs
45 in cells infected with influenza virus at low MOI. We find extremely large variation in the amount
46 of viral mRNA expressed in individual cells. Both co-infection and activation of innate-immune
47 pathways are rare in our low-MOI infections, and do not appear to be the major drivers of cell-
48 to-cell heterogeneity in viral transcriptional load. Individual infected cells often fail to express
49 specific viral genes, and such gene absence explains some but certainly not all of the cell-to-cell
50 heterogeneity. A variety of cellular genes, including ones involved in the oxidative-stress response,
51 co-vary with viral transcriptional load. Overall, our work demonstrates remarkable heterogeneity in
52 the transcriptional outcome of influenza virus infection among nominally identical cells infected
53 with a relatively pure population of virions.

54 Results

55 Strategy to measure mRNA in single virus-infected cells.

56 We performed single-cell mRNA sequencing using a droplet-based system that physically isolates
57 individual cells prior to reverse transcription ([Zheng et al., 2017; Macosko et al., 2015; Klein et al., 2015](#)).
58 Each droplet contains primers with a unique *cell barcode* that tags all mRNAs from that
59 droplet during reverse-transcription. Each primer also contains a *unique molecular identifier (UMI)*
60 that is appended to each mRNA molecule during reverse transcription. The 3' ends of the mRNAs are
61 sequenced and mapped to the human and influenza virus transcriptomes to determine transcript
62 identities. This information is combined with that provided by the UMIs and cell barcodes to

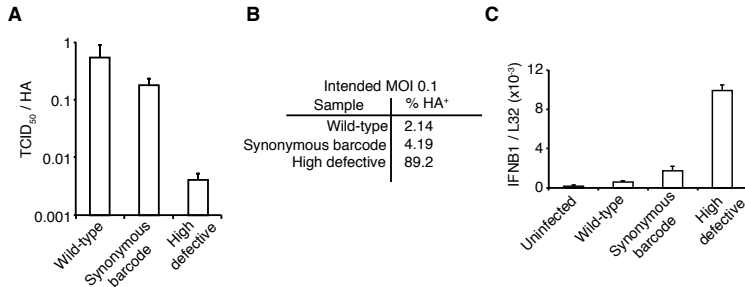


Figure 2. The viral stocks in our experiments are relatively pure of defective particles. **(A)** Our viral stocks have a higher ratio of infectious particles to HA virion RNA compared to a high-defective stock propagated at high MOI. HA viral RNA was quantified by qPCR on virions. Error bars \pm S.D., n=6 (qPCR replicates). **(B)** Our viral stocks have a higher ratio of infectious particles to particles capable of expressing HA protein. A549 cells were infected at an MOI of 0.1, and the percentage of cells expressing HA protein at 9 hours post-infection was quantified by antibody staining and flow cytometry. **(C)** Our viral stocks are less immunostimulatory than virus propagated at high MOI. Measurements of *IFNB1* transcript by qPCR normalized to the housekeeping gene L32 in A549 cells at 10 hours post infection at an MOI of 0.5. Error bars \pm S.D., n=3. Note that MOIs were calculated by TCID50 on MDCK-SIAT1 cells, whereas the experiments in this figure involved infection of A549 cells.

Figure 2-Figure supplement 1. Full flow cytometry data for panel B .

63 quantify the number of molecules of each mRNA species that have been captured for each cell.
 64 Infected cells will express viral as well as cellular mRNAs – however the cell barcodes and UMs
 65 cannot distinguish whether a cell was initially infected by one or multiple viral particles. We therefore
 66 engineered an influenza virus (strain A/WSN/1933) that additionally carried *viral barcodes* consisting
 67 of synonymous mutations near the 3' end of each transcript (Figure 1A). Critically, these synonymous
 68 mutations did not greatly impact viral growth kinetics (Figure 1B). We infected A549 human lung
 69 carcinoma cells with an equal mix of the wild-type and synonymously barcoded viruses. Cells
 70 infected by a single virion will exclusively express mRNAs from either wild-type or synonymously
 71 barcoded virus, whereas cells that are co-infected with multiple virions will often express mRNAs
 72 from both the wild-type and synonymously barcoded viruses (Figure 1C).

73 We took care to generate stocks of virus that were relatively “pure” of defective particles.
 74 Stocks of viruses typically contain an array of biologically active viral particles, some of which are
 75 defective for replication owing to mutations or deletions in essential viral genes (*von Magnus, 1954;*
Huang et al., 1970; Brooke, 2014; Fonville et al., 2015; Lauring and Andino, 2010; Dimmock et al., 2014; Saira et al., 2013). These defective particles become prevalent when a virus is grown at
 76 high MOI, where complementation permits the growth of otherwise deleterious genotypes. To
 77 minimize the levels of defective particles, we propagated our viral stocks at low MOI for a relatively
 78 brief period of time (*Xue et al., 2016*). We validated that our stocks exhibited greater purity of
 79 infectious particles than a stock propagated at high MOI by verifying that they had a higher ratio
 80 of infectious particles to virion RNA (Figure 2A) and to particles capable of inducing expression of
 81 a single viral protein (Figure 2B). In addition, viral stocks with many defective particles are more
 82 immunostimulatory (*Tapia et al., 2013; Lopez, 2014*). We confirmed that our viral stocks induced
 83 less interferon than a stock propagated at higher MOI (Figure 2C).

86 Single cells show an extremely wide range of expression of viral mRNA.

87 We infected A549 cells at low MOI with a mixture of the wild-type and synonymously barcoded
 88 viruses, and collected cells for sequencing at 6, 8, and 10 hours post-infection, including a replicate
 89 a 8-hours. We replaced the infection inoculum with fresh media at one-hour post-infection, thereby
 90 ensuring that most infection was initiated during a narrow time window. The exception was the
 91 replicate 8-hour sample, for which we did *not* perform this media change and instead left the

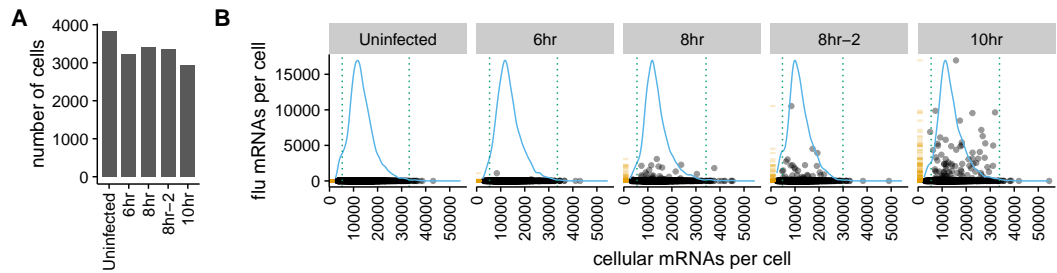


Figure 3. There is a very wide distribution in the amount of viral mRNA per cell. **(A)** Number of cells sequenced for each sample. **(B)** The number of cellular and viral mRNAs detected for each cell is plotted as a point. The blue lines show the overall distribution of the number of cellular mRNAs per cell. The orange rug plot at the left of each panel shows the distribution of the number of viral mRNAs per cell. Cells outside the dotted green lines were considered outliers with suspiciously low or high amounts of cellular mRNA (possibly derived from two cells per droplet), and were excluded from all subsequent analyses.

92 cells in the original infection inoculum. We recovered between 3,000 and 4,000 cells for each
 93 sample (Figure 3A). As expected for a low-MOI infection, most cells expressed little or no viral mRNA
 94 (Figure 3B). Also as expected, the amount of viral mRNA per cell among infected cells increased over
 95 time (Figure 3B). But what was most notable was how widely the number of viral mRNA molecules
 96 varied among infected cells. While the fraction of mRNA derived from virus was <0.1% for most
 97 cells, viral mRNA constituted half the transcriptome in a few cells at 8 and 10 hours (Figure 3B).

98 A complicating factor is that uninfected cells could have small amounts of viral mRNA due
 99 to leakage of transcripts from lysed cells. It is therefore important to establish a threshold for
 100 identifying truly infected cells. We can do this by taking advantage of the fact that roughly half the
 101 infecting virions bear synonymous barcodes. Reads derived from lysed cells will be drawn from
 102 both wild-type and synonymously barcoded viral transcripts. However, most cells are infected by at
 103 most one virion, and so the reads from truly infected cells will usually derive almost entirely from
 104 one of the two viral variants. Figure 4A shows the fraction of viral reads in individual cells from each
 105 viral variant, and Figure 4B indicates the fraction of viral reads from the most abundant variant in
 106 that cell. Most cells with large amounts of viral mRNA have viral transcripts exclusively derived from
 107 one viral variant – indicating non-random partitioning as expected from viral infection. However,
 108 cells with a small amount of viral mRNA often have viral transcripts from both variants, as expected
 109 from the random partitioning associated with simple mRNA leakage. Finally, a few cells with large
 110 amounts of viral mRNA have viral transcripts from both variants, reflecting co-infection.

111 We determined the threshold amount of viral mRNA per cell at which the barcode partitioning
 112 clearly resulted from infection rather than leakage (Figure 4C), and used this threshold to annotate
 113 cells that we were confident were truly infected. We also annotated as co-infected cells above this
 114 threshold that had mRNA from both viral variants. Figure 4D shows the number of cells annotated
 115 as infected and co-infected for each sample – these cells are just a small fraction of the number of
 116 cells with any viral read. These annotation thresholds are conservative, and will miss some true
 117 low-level infections, as well as any co-infections with the same viral variant. However, it is important
 118 that the analyses below are restricted to cells that are truly infected with virus, so we accepted
 119 the loss of some low-level infections in order to avoid false positives. Because most cells are not
 120 infected, we subsampled the uninfected cells to the numbers shown in Figure 4D to balance the
 121 proportions of infected and uninfected cells for all subsequent analyses.

122 Strikingly, the extreme variation in the number of viral transcripts per cell remains even after we
 123 apply these rigorous criteria for annotating infected cells (Figure 4E). The fraction of viral mRNA per
 124 infected cell follows a roughly exponential distribution, with many cells having few viral transcripts
 125 and a few cells having many. At 6 and 8 hours <10% of infected cells are responsible for over half
 126 the viral transcripts, while at 10 hours ≈15% of infected cells produce over half the viral transcripts

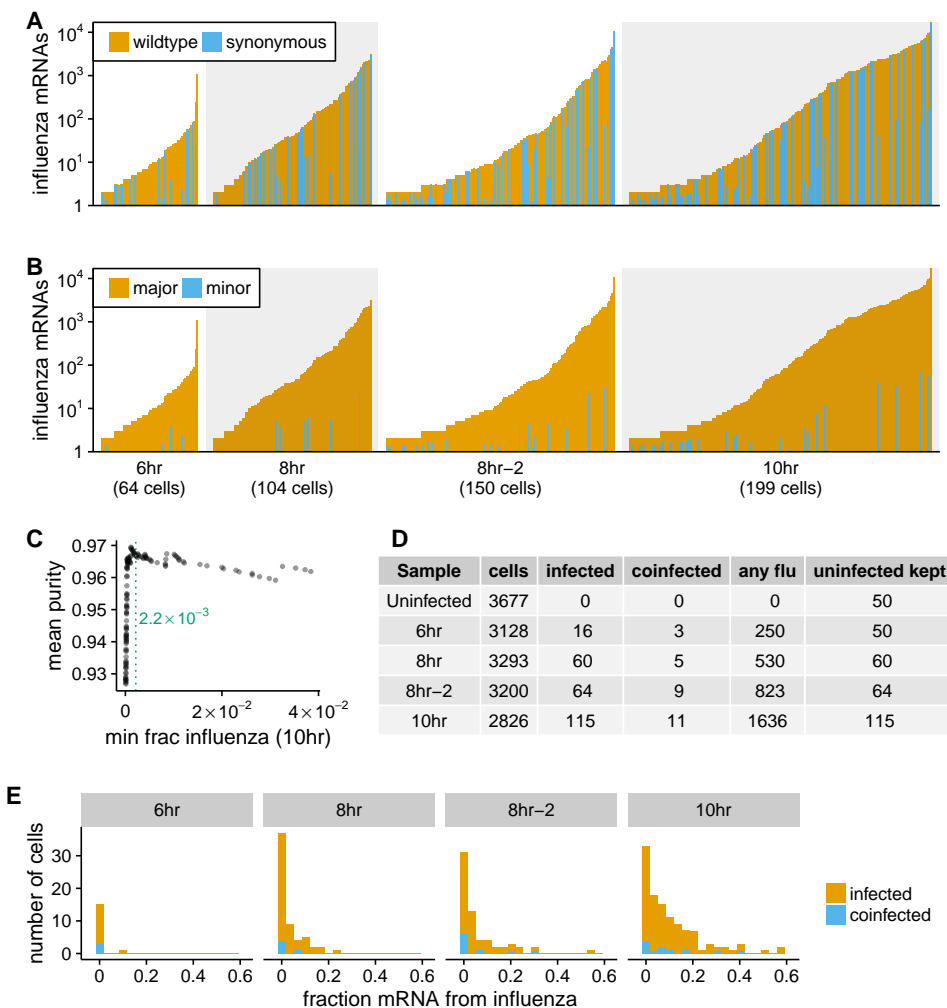


Figure 4. Synonymous barcodes on the viral mRNAs distinguish true infections from cells that contain viral mRNAs derived from leakage of lysed cells. **(A)** Cells with at least two viral mRNAs for which the barcode could be called, arranged in order of increasing influenza transcript counts. Bar heights denote the number viral mRNAs on a \log_{10} scale, bar coloring is linearly proportional to the fractions of viral mRNAs derived from wild-type and synonymously barcoded virus. **(B)** Same as (A), but each bar is colored according to the relative fraction of the more common (major) and less common (minor) virus variant. At low levels of viral mRNA there is often a roughly equal mix, suggesting contamination with viral mRNAs leaked from lysed cells. At higher levels of viral mRNA, cells generally have only one viral variant, suggesting infection initiated by a single virion. A few cells are also obviously co-infected with both viral variants. **(C)** We determined a cutoff for calling “true” infections by finding the amount of viral mRNA per cell at which the viral barcode purity no longer increases with more viral mRNA. The purity is the fraction of all viral mRNA in a cell derived from the most abundant viral barcode in that cell. We fit a curve to the mean purity of all cells with more than the indicated amount of viral mRNA, and drew the cutoff at the point where this curve stopped increasing with the fraction of total mRNA derived from virus. See the Methods for details. **(D)** The number of cells identified as infected and co-infected for each sample, as well as the number of cells with any viral read. For all subsequent analyses, we subsampled the number of uninfected cells per sample to the greater of 50 or the number of infected cells. **(E)** Distribution of the fraction of mRNA per cell derived from virus for both infected and co-infected cells.

Figure 4-Figure supplement 1. Number of viral barcodes called.

Figure 4-Figure supplement 2. Fraction of total viral mRNA derived from a given fraction of infected cells.

127 (Figure 4-Figure supplement 2). Notably, co-infected cells do not express dramatically more viral
 128 mRNA than other cells (Figure 4), suggesting that the initial infectious dose is not the major driver
 129 of cell-to-cell variation in our low-MOI infections.

130 **Absence of viral genes partially explains cell-to-cell variability in viral load.**

131 The influenza genome is segmented, and cells can fail to express a viral mRNA if the encoding
132 gene segment is not packaged in the infecting virion or fails to initiate transcription after infection.
133 Indeed, several groups have reported that the majority of infected cells fail to express at least
134 one viral gene (*Brooke et al., 2013; Heldt et al., 2015; Dou et al., 2017*). We wondered if the
135 absence of specific viral genes might be associated with reduced amounts of viral mRNA within
136 single infected cells. In particular, transcription of influenza virus mRNAs is performed by the viral
137 ribonucleoprotein (RNP) complex, which consists of the three proteins that encode the tripartite
138 polymerase (PB2, PB1, and PA) as well as nucleoprotein (NP) (*Huang et al., 1990*). Each viral gene
139 segment is associated with one RNP in incoming infecting virions, but secondary transcription by
140 newly synthesized RNPs requires the presence of the viral genes encoding each of the four RNP
141 proteins (*Vreede et al., 2004; Eisfeld et al., 2015*). This secondary transcription is a major source
142 of viral mRNAs, as evidenced by the fact that blocking synthesis of the RNP proteins reduces the
143 amount of viral mRNA by several orders of magnitude in bulk cells (Figure 5-Figure supplement 1).

144 We examined the total amount of viral mRNA versus the expression of each viral gene (Figure 5A,
145 Figure 5-Figure supplement 2). Cells that lack an RNP gene never derive more than a few percent of
146 their mRNAs from virus, confirming the expected result that all four RNP genes are essential for
147 high levels of viral transcription. However, we observe cells that lack each of the other non-RNP
148 genes but still derive \approx 40% of their mRNAs from virus, suggesting that none of the other genes are
149 important for high levels of viral transcription. These results are statistically supported by Figure 5B,
150 which shows that absence of any RNP gene but *not* any other viral gene is associated with reduced
151 amounts of viral mRNA. However, gene absence clearly does not explain all of the variability in viral
152 gene expression, since even cells expressing all viral genes exhibit a very wide distribution in the
153 amount of viral mRNA that they express. Specifically, at both 8 and 10 hours, the amount of viral
154 mRNA in individual cells expressing all eight viral genes still ranges from <1% to >50% (Figure 5A,
155 Figure 5-Figure supplement 2).

156 We also quantified the fraction of infected cells that completely failed to express a given gene. We
157 limited this analysis to examining the presence / absence of the non-RNP genes in cells expressing
158 all four RNP genes, since we might fail to detect viral transcripts that are actually present at low
159 levels in RNP-deficient cells due to the lower viral burden in these cells. At the 8- and 10-hour time
160 points, between 5% and 17% of cells fail to express any one of the four non-RNP genes (Figure 5C).
161 The absence of a given gene appears to be an independent event, as the probability of observing
162 all four non-RNP genes in a cell is well predicted by simply multiplying the probabilities of observing
163 each gene individually (Figure 5C). If we extrapolate the frequencies at which cells lack non-RNP
164 genes to the RNP genes, then we would predict that 40-50% of infected cells express mRNAs from
165 all eight genes. This estimate of the frequency at which infected cells express mRNAs from all eight
166 gene segments is slightly higher than previous estimates of 13% (*Brooke et al., 2013*) and 20% (*Dou*
167 *et al., 2017*). At least one difference is that *Brooke et al. (2013)* stained for proteins whereas we
168 examined the expression of mRNAs – it is likely that some cells contain mutated viral genes that fail
169 to produce stable protein even when mRNA is expressed.

170 **The relative amounts of different viral mRNAs are more consistent across cells.**

171 The results above show that the amount of viral mRNA in infected cells varies over several orders
172 of magnitude. Does the relative expression of viral genes exhibit similar cell-to-cell variability?
173 To address this question, we focused on cells that derived >5% of their mRNA from virus, since
174 estimates of relative viral gene expression will be less noisy in cells with more viral mRNAs.

175 In contrast to the extreme variability in the total viral mRNA per cell, the fraction of this mRNA
176 derived from each gene is much more consistent across cells (Figure 6A). Total viral mRNA varies by
177 orders of magnitude, but the fraction from any given viral gene is fairly tightly clustered around the
178 median value for all cells (Figure 6B). The relative levels of each viral mRNA in our cells are similar
179 to prior bulk measurements made by Northern blots (*Hatada et al., 1989*), which also found an

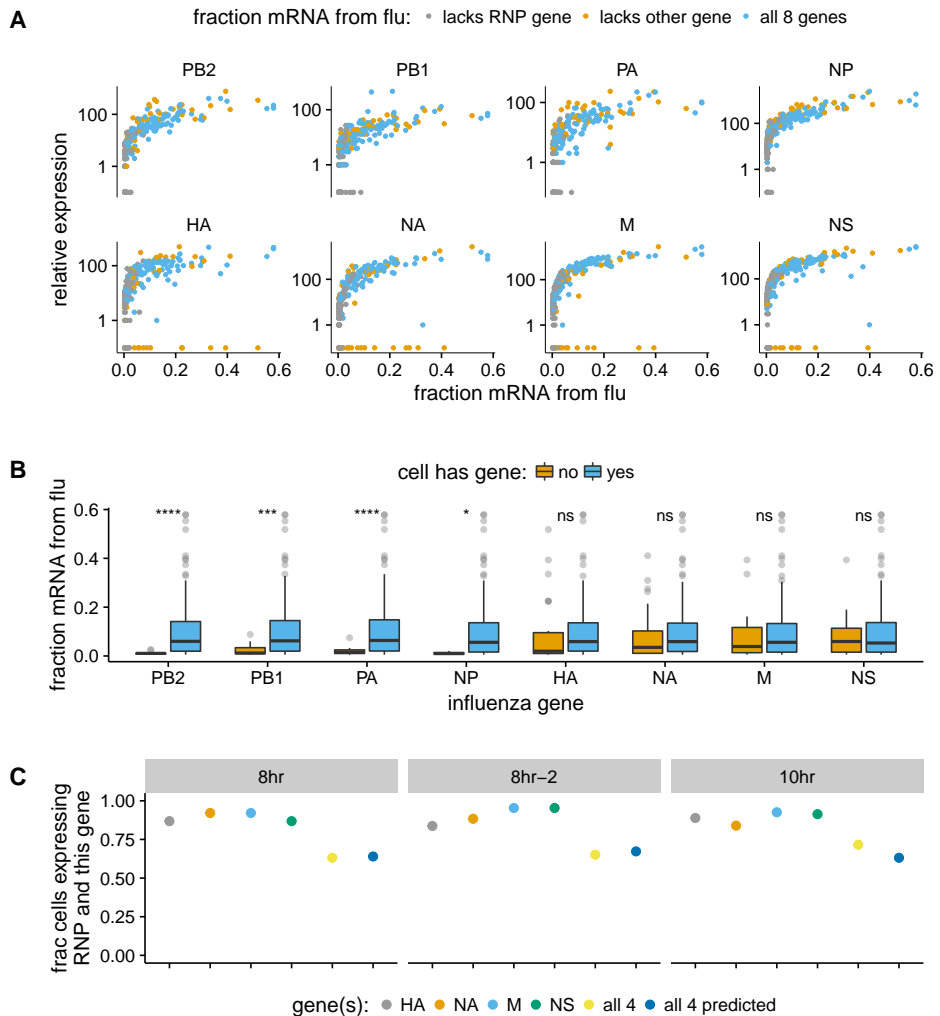


Figure 5. The absence of viral genes explains some of the variability in the amount of viral mRNA per cell. **(A)** Fraction of mRNA in each infected cell derived from virus as a function of the normalized expression of each viral gene in that cell, taken over all time points. Cells with high viral burden always express all RNP genes, but some cells with high viral burden lack each of the other genes. **(B)** Box and whisker plots showing the per-cell viral burden among cells with >0.5% of their mRNA from virus, binned by whether or not the cells express each gene. A Wilcoxon signed-rank test was used to test the null hypothesis that absence of each gene does not affect viral burden: **** = $P < 10^{-4}$, *** = $P < 10^{-3}$, * = $P < 0.05$, ns = not significant. **(C)** The fraction of cells that express each of the four other genes among cells that express all RNP genes, as well as the fraction that express *all* four of the other genes. The fraction that express *all* four genes is well predicted by simply multiplying the frequencies of cells that express each gene individually, indicating that gene absence is approximately independent across these genes.

Figure 5-Figure supplement 1. Secondary transcription is a major source of viral mRNA during bulk infections.

Figure 5-Figure supplement 2. Like panel (A), but shows samples individually.

Figure 5-Figure supplement 3. Like panel (B) but for the 10-hr sample only.

Figure 5-source data 1. The numerical data for panel (C) are in `p_missing_genes.csv`.

180 expression hierarchy of M > NS > NP > NA > HA > PB2 ~ PB1 ~ PA. The cell-to-cell consistency in
 181 the relative expression of different viral genes is even tighter if we limit the analysis only to cells
 182 that express all eight viral genes (Figure 6C,D). Therefore, with the exception of complete gene
 183 absence, the factors that drive the dramatic cell-to-cell variability in the amount of viral mRNA
 184 have roughly similar effects on all viral genes in a given cell. This finding is consistent with prior

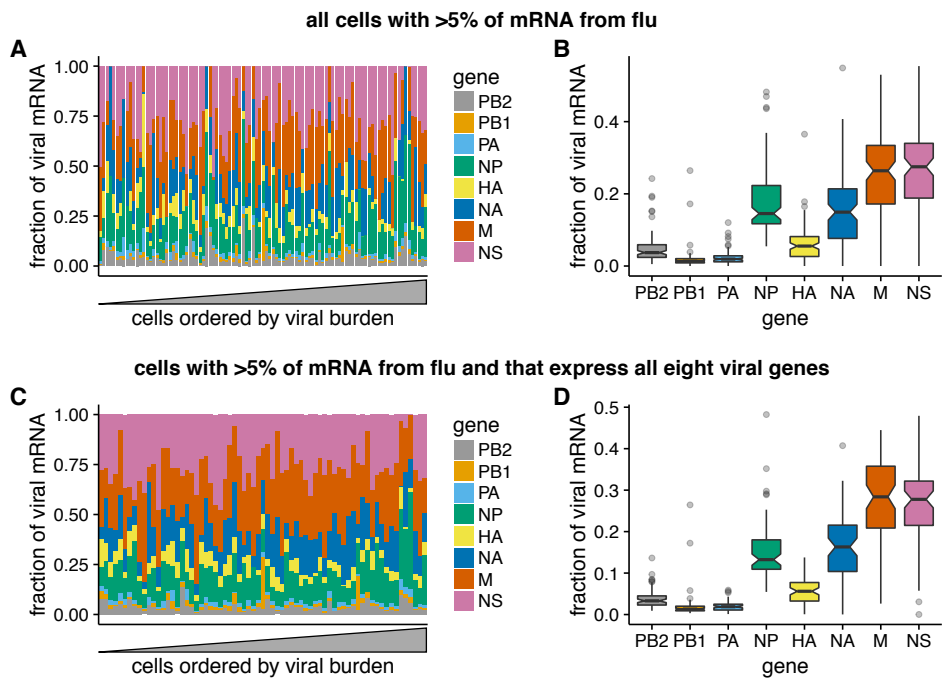


Figure 6. Relative expression of influenza virus genes in highly infected cells (>5% of total mRNA from virus). **(A)** The fraction of viral mRNA from each viral gene for each cell. **(B)** Box plots showing the distribution of the fraction of viral mRNA per cell from each viral gene. The black lines at the notches are the medians, and the tops and bottoms of boxes indicate the first and third quartiles. Whiskers extend to the highest or lowest data point observed within 1.5x the interquartile range, outliers shown as circles. Notches extend 1.58x the interquartile range divided by the square root of the number of observations. **(C), (D)** The same plots, but only including cells for which we observed at least one molecule of each viral gene.

Figure 6-source data 1. The raw data are in `p_fiu_expr.csv`.

work showing positive correlations among the abundance of several viral genome segments in individual cells ([Heldt et al., 2015](#)). It is also reminiscent of the observation that total cellular mRNA varies among single cells as a function of factors such as volume that affect all mRNA species concordantly ([Padovan-Merhar et al., 2015](#)).

189 **Co-infection can provide infected cells with the full complement of viral genes.**

190 Our sequencing enables us to identify the rare cells that were co-infected with both wild-type and
 191 synonymously barcoded viral variants. Overall, we captured 10 such co-infected cells that had >5%
 192 of their mRNA derived from virus (Figure 7). Seven of these 10 cells expressed all eight viral genes.
 193 Remarkably, the majority (4 of 7) of these cells would *not* have expressed all the viral genes in the
 194 absence of co-infection, since they have at least one gene exclusively derived from each viral variant.
 195 For instance, the cell with 11.2% of its mRNA from virus in the upper right of Figure 7 expresses
 196 M only from the wildtype viral variant, and NP and HA only from the synonymously barcoded
 197 variant. Our data therefore provide direct single-cell support for the idea that co-infection can
 198 rescue missing viral genes ([Brooke et al., 2013, 2014; Fonville et al., 2015; Aguilera et al., 2017](#)).

199 Another observation from Figure 7 is that co-infected cells usually express roughly equal
 200 amounts of transcripts from each of the two viral variants. This observation is consistent with the
 201 finding by [Dou et al. \(2017\)](#) and [Huang et al. \(2008\)](#) that the temporal window for co-infection is
 202 short – if both viral variants infect a cell at about the same time, then neither will have a headstart
 203 and so each will have a roughly equal opportunity to transcribe its genes.

204 To support this idea with a larger dataset albeit at lower resolution, we generated a virus
 205 in which the HA coding sequence was replaced by GFP. We then co-infected cells with a mix of

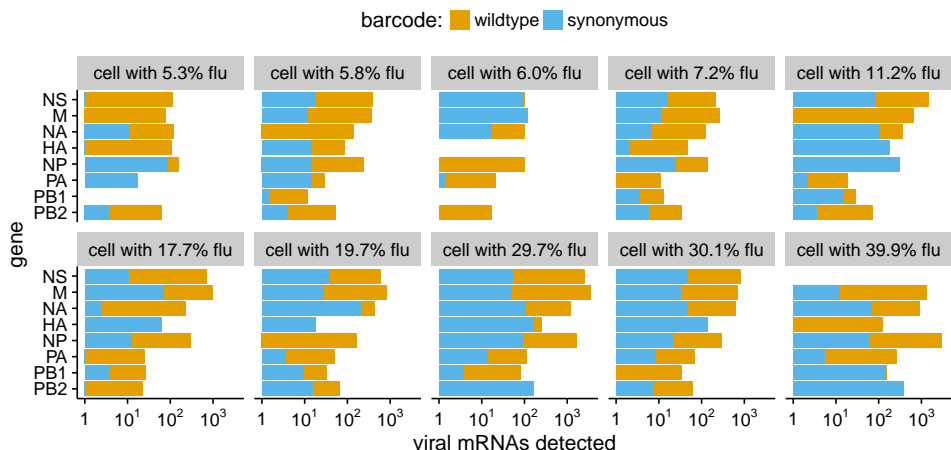


Figure 7. The abundance of each viral transcript in cells that are co-infected with the two viral variants and have >5% of their mRNA derived from virus. The bars show the logarithms of the numbers of each viral mRNA detected, and are colored in linear proportion to the fraction of that mRNAs derived from wild-type or synonymously barcoded virus.

Figure 7-Figure supplement 1. Co-infected cells express roughly equal amounts of a gene from each infecting viral variant.

Figure 7-source data 1. The raw data plotted in this figure are in `p_co-infection.csv`.

Figure 7-source data 2. The sequence of the HA viral RNA carrying the GFP gene is in `HAflank-eGFP.fasta`.

206 wildtype and Δ HA-GFP virus and used flow cytometry to score cells for the presence of HA only
 207 (infection by wildtype virus), GFP only (infection by Δ HA-GFP virus), or both (co-infection) as shown
 208 in Figure 7 Figure supplement 1. As in our single-cell sequencing data, we found that expression
 209 of HA and GFP were highly correlated, indicating that co-infected cells typically expressed roughly
 210 equal amounts of transcript from each viral variant.

211 **Activation of the interferon response is rare in single infected cells.**

212 Because our sequencing captured all polyadenylated transcripts, we can examine whether there
 213 are prominent changes in the host-cell transcriptome in sub-populations of infected cells. Influenza
 214 virus infection can trigger innate-immune sensors that lead to the transcriptional induction of
 215 type I and III interferons, and subsequently of anti-viral interferon-stimulated genes (*Killip et al.,*
216 2015; Iwasaki and Pillai, 2014; Crotta et al., 2013). However, activation of the interferon response
 217 is stochastic and bi-modal at the level of single cells (*Chen et al., 2010; Shalek et al., 2013, 2014;*
218 Perez-Cidoncha et al., 2014; Bhushal et al., 2017; Hagai et al., 2017). We therefore hypothesized
 219 that we might see two sub-populations of infected cells: one in which the interferon response
 220 inhibited viral transcription, and another in which the virus was able to express high levels of its
 221 mRNA by evading or blocking this response.

222 To examine whether there were distinct sub-populations of virus-infected cells, we used a
 223 semi-supervised t-SNE approach (*Van der Maaten and Hinton, 2008*) to cluster cells by genes that
 224 co-varied with viral infection status. As shown in Figure 8A,B, this approach effectively grouped cells
 225 by the amount of viral mRNA that they expressed. Sample-to-sample variation was regressed away
 226 during the clustering, as cells did not obviously group by time-point, with expected exception that
 227 the uninfected and 6-hour samples had few cells in the region of the plot corresponding to large
 228 amounts of viral mRNA (Figure 8C).

229 But to our surprise, we did not see a prominent clustering of infected cells into sub-populations
 230 as expected if the interferon response was strongly activated in some cells. To investigate fur-
 231 ther, we annotated each cell by the total number of type I and III interferon transcripts detected.
 232 Remarkably, only a single cell expressed detectable interferon (Figure 8D). We also examined

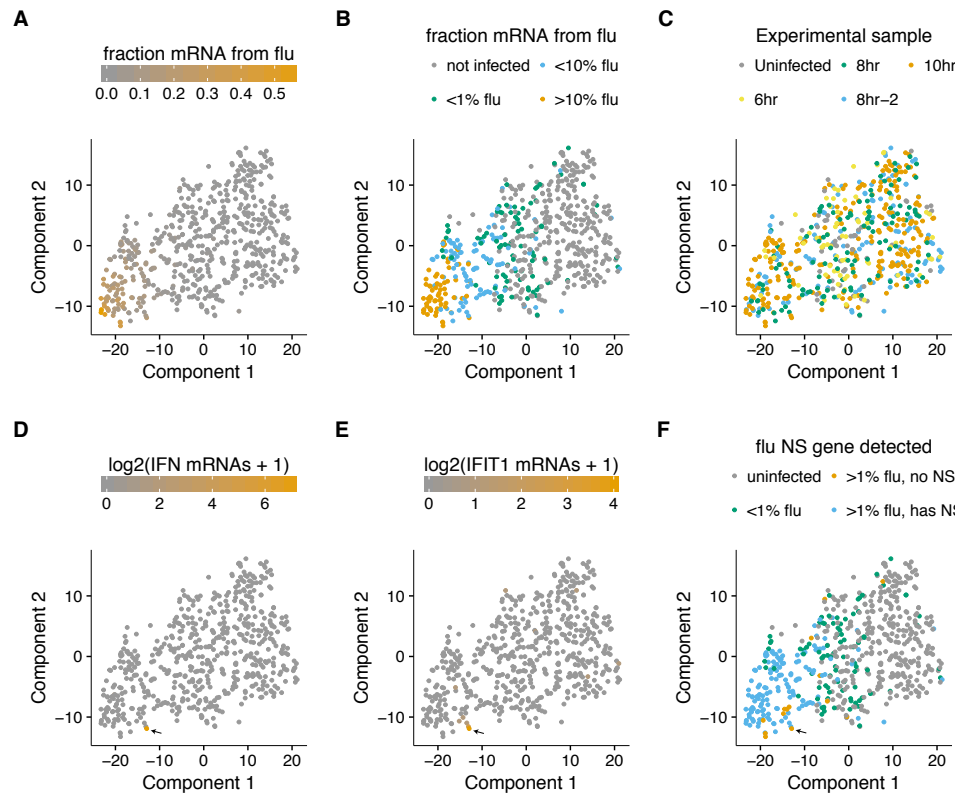


Figure 8. A t-SNE plot created by semi-supervised clustering using genes that co-vary with viral infection status. Each point is a single cell, and each panel shows an identical layout but colors the cells according to a different property. **(A), (B)** Cells colored by the fraction of their mRNA derived from virus. **(C)** Cells colored by the experimental sample. **(D), (E)** Cells colored by the number of detected transcripts from type I and III interferons (IFN). Only one cell has detectable interferon expression (in orange, indicated with arrow). **(F)** Cells colored by the expression of the interferon-stimulated gene IFIT1. **(F)** Cells colored by whether they express the viral NS gene. The one interferon-positive cell is lacking NS, but so are many interferon-negative cells.

interferon-stimulated genes, which are induced by autocrine and paracrine interferon signaling. Figure 8E shows expression of one such gene, IFIT1 (*Fensterl and Sen, 2011*). As with interferon itself, expression of IFIT1 was rare and most prominent in the single interferon-positive cell, presumably due to the higher efficiency of autocrine versus paracrine signaling. Notably, interferon and interferon-stimulated genes were also relatively ineffective at blocking viral transcription in the single cell in which they were potently induced, since >10% of the mRNA in this cell was derived from virus (Figure 8A,B,D,E).

We posited that the paucity of interferon induction might be due to the activity of influenza virus's major interferon antagonist, the NS1 protein (*García-Sastre et al., 1998; Hale et al., 2008*). We therefore identified cells that expressed substantial amounts of viral mRNA but lacked the NS gene (Figure 8F). Consistent with the idea that NS1 is important for suppressing interferon, the one interferon-positive cell lacked detectable expression of the NS gene. But other cells that lacked NS expression still failed to induce a detectable interferon response, despite often having a substantial amount of their mRNA derived from virus (Figure 8). This result is in line with other work showing that NS1-deficient influenza virus does not deterministically induce interferon (*Killip et al., 2017; Kallfass et al., 2013*). Therefore, many individual infected cells fail to activate innate-immune responses even when the virus lacks its major interferon antagonist.

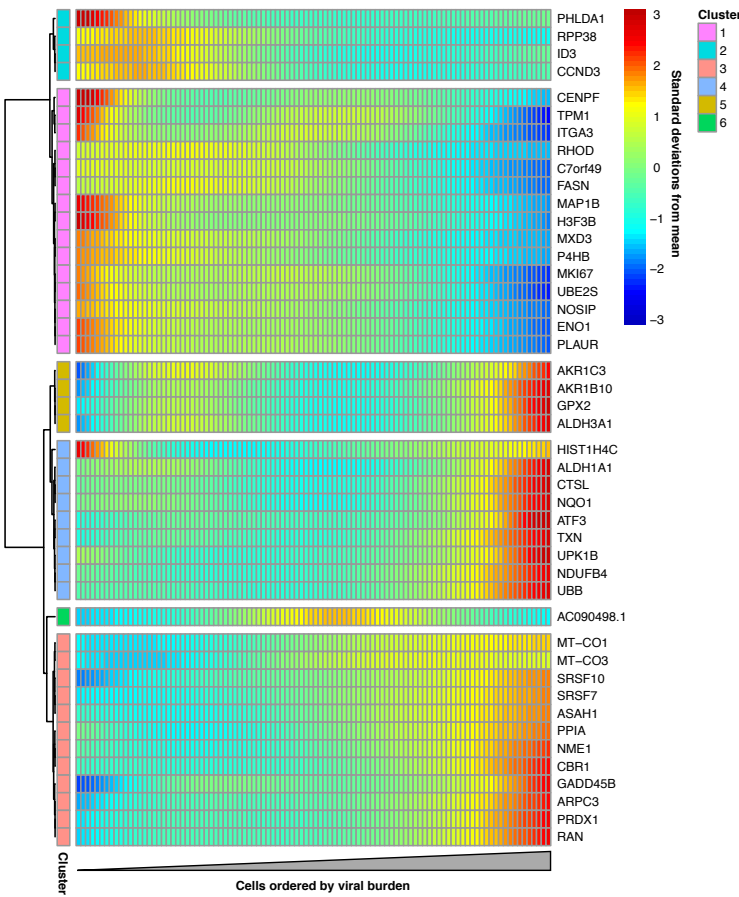


Figure 9. Cellular genes that co-vary in expression with the amount of viral mRNA in cells expressing all eight viral genes. The columns are cells, ordered from left to right by the fraction of mRNA derived from virus. Each row is a gene that is differentially expressed as a function of the fraction of mRNA derived from virus at a false discovery rate of 0.1. Genes for which the color goes from blue at left to red at right are expressed at higher levels in cells with more viral mRNA. The scale bar indicates the number of standard deviations above or below the mean expression, truncated at 3-fold on both sides.

Figure 9-source data 1. The full results of the differential expression test is in `p_sig_cellular_genes.csv`.

Figure 9-source data 2. The results of a gene-set analysis are in `p_sig_cellular_genes.csv`.

Figure 9-Figure supplement 1. Many genes that co-vary with viral load are involved in the oxidative stress response.

250 Some host genes co-vary with viral gene expression.

251 We examined whether any host genes were differentially expressed in cells with more viral mRNA.
 252 We restricted this analysis to infected cells with all eight viral genes in order to focus on cellular
 253 genes that were associated with viral mRNA burden independent of effects due to the presence or
 254 absence of particular viral transcripts. We identified 45 cellular genes that co-varied with viral gene
 255 expression at a false discovery rate of 0.1 (Figure 9).

256 Many of the genes with increased expression in cells with more viral mRNA are known or
 257 suspected to be regulated by the Nrf2 master regulator in response to oxidative stress. These genes
 258 produce proteins that are involved in detoxification of reactive oxygen species or resultant products,
 259 the management of misfolded proteins, the electron transport chain, or a general stress response
 260 (Figure 9-Figure supplement 1). We additionally see reduced expression of the nitric oxide synthase
 261 interacting protein (NOSIP). Transient oxidative stress is known to occur during viral infection, and
 262 may act in a proviral fashion via MAPK activation driving vRNP export (*Amatore et al., 2014*). The
 263 antioxidant response is thought to be largely antiviral, potentially through inhibition of MAPK activity

264 (*Lin et al., 2016; Sgarbanti et al., 2014*). Our data do not reveal whether the expression of genes
265 involved in the response to oxidative stress are a cause or a symptom of higher levels of viral mRNA,
266 and further investigation of this topic is an interesting area for future work.

267 Discussion

268 We have quantified the total transcriptome composition of single cells infected with influenza virus.
269 While we observe a general increase in the amount of viral mRNA over time as expected from
270 bulk measurements (*Hatada et al., 1989; Shapiro et al., 1987*), there is wide variation in viral gene
271 expression among individual infected cells.

272 The most obvious form of heterogeneity is the complete failure of some infected cells to express
273 one or more viral genes, which we estimate occurs in about half the infected cells in our experiments.
274 The absence of some viral genes in some infected cells has been noted previously (*Brooke et al.,
275 2013; Heldt et al., 2015; Dou et al., 2017*), and our work provides a holistic view by quantifying the
276 total viral transcriptional load as a function of the level of each mRNA. We find that cells lacking
277 expression of any of the four genes that encode the viral RNP express much less total viral mRNA,
278 consistent with prior bulk studies (*Vreede et al., 2004; Eisfeld et al., 2015*). Interestingly, the reason
279 some cells fail to express some viral genes remains unclear. The prototypical influenza virion
280 packages one copy of each of the eight gene segments (*Noda et al., 2006; Hutchinson et al., 2010*),
281 but some virions surely package fewer (*Brooke et al., 2014*). However, it is also possible that much
282 of the viral gene absence is due to stochastic loss of viral RNPs after infection but prior to the
283 initiation of viral transcription in the nucleus.

284 The absence of viral genes only partially explains the cell-to-cell variation in amount of viral
285 mRNA, which still varies from <1% to >50% among cells expressing all the viral genes. It is likely
286 that other viral genetic factors explain some of this remaining heterogeneity. The 3'-end sequencing
287 strategy used in our experiments detects the presence of a viral gene, but does not identify
288 whether that gene contains a mutation that might hinder viral replication. However, viral mutations
289 are also unlikely to explain all the observed heterogeneity, since current consensus estimates of
290 influenza virus's mutation rate suggest that the typical virion in a stock such as the one used in our
291 experiment should contain less than one mutation per genome (*Parvin et al., 1986; Suárez et al.,
292 1992; Suárez-López and Ortín, 1994; Nobusawa and Sato, 2006; Bloom, 2014; Pauly et al., 2017*).

293 The rest of the heterogeneity must be due to some combination of cellular factors and inherent
294 stochasticity. Some features of the cellular transcriptome co-vary with the amount of influenza
295 mRNA. In particular, the viral load in individual cells is associated with the expression of genes
296 involved in response to cellular stresses, including oxidative stress. It will be interesting to determine
297 if these cellular transcriptional signatures are simply a consequence of the stress imposed by viral
298 replication, or if their stronger activation in some cells is a causative factor that promotes viral
299 transcription. However, it also would not be surprising if a substantial amount of the cell-to-cell
300 heterogeneity cannot be ascribed to pre-existing features of either the viral genome or cellular state.
301 Apparently stochastic heterogeneity is a common feature of many processes at a single-cell level (*Cai
302 et al., 2006; Raj et al., 2006; Buganim et al., 2012; Shalek et al., 2013; Avraham et al., 2015*) –
303 especially when those processes are initiated by very small numbers of initial molecules (*Elowitz
304 et al., 2002*), as is the case for low-MOI viral infection.

305 Our data do suggest that the factors driving the heterogeneity in viral transcriptional load exert
306 relatively concordant effects on all viral genes in a given cell. Specifically, despite the extreme
307 heterogeneity in total viral mRNA per cell, the relative levels of the viral mRNAs are reasonably
308 consistent across cells, and generally reflective of classical bulk measurements (*Hatada et al., 1989*).
309 Therefore, despite the stochasticity inherent in initiating transcription and replication of each gene
310 from a single copy carried by the incoming virion, as long as a gene is not completely lost then the
311 virus possesses mechanisms to control its relative expression (*Shapiro et al., 1987; Hatada et al.,
312 1989; Perez et al., 2010; Heldt et al., 2012; Chua et al., 2013*).

313 One factor that surprisingly does *not* appreciably contribute to the heterogeneity in our ex-
314 periments is activation of innate-immune interferon pathways. Only one of the hundreds of
315 virus-infected cells expresses any detectable interferon, despite the fact that a number of cells fail
316 to express the influenza-virus interferon antagonist NS1. It is known that interferon activation is
317 stochastic at the level of single cells in response to both synthetic ligands (*Shalek et al., 2013, 2014;*
318 *Bhushal et al., 2017; Hagai et al., 2017*) and actual infection (*Rand et al., 2012; Perez-Cidoncha*
319 *et al., 2014; Avraham et al., 2015; Killip et al., 2017*). But interferon expression is a prominent
320 transcriptional signature of high-MOI influenza virus infection of bulk cells, including in the epithelial
321 cell line and at the time-points used in our experiments (*Geiss et al., 2002; Sutejo et al., 2012*). So
322 it is notable how rarely single cells express interferon. Interferon expression would surely be more
323 common at later times or with a viral stock passaged at higher MOI, since paracrine interferon
324 signaling (*Crotta et al., 2013*) and accumulation of defective viral particles enhance innate-immune
325 detection (*Tapia et al., 2013; Lopez, 2014*). However, the early events of physiological influenza
326 infection involve just a few virions (*Varble et al., 2014; McCrone et al., 2017*), and so it is interesting
327 to speculate whether rare events such as interferon activation during the first few cycles of viral
328 replication could contribute to heterogeneity in the eventual outcome of infection.

329 Overall, our work shows the power and importance of charactering cellular infection at the level
330 of single cells (*Avraham et al., 2015*). The dynamics of viral infection in any given cell is shaped
331 by the genetic composition of the incoming virion, the host-cell state, the bi-modality of innate-
332 immune activation, and the inherent stochasticity of molecular processes initiated by a single copy
333 of each viral gene. We have shown how the confluence of these factors leads to extreme cell-to-cell
334 heterogeneity in the transcriptional outcome of influenza virus infection. Further deconstruction of
335 the contributions of each factor will enable a deeper understanding of how the bulk features of
336 infection emerge from the processes occurring within individual virus-infected cells.

337 Methods and Materials

338 Cell lines and viruses

339 The following cell lines were used in this study: the human lung epithelial carcinoma line A549
340 (ATCC CCL-185), the MDCK-SIAT1 variant of the Madin Darby canine kidney cell line overexpressing
341 human SIAT1 (Sigma-Aldrich 05071502), and the human embryonic kidney cell line 293T (ATCC
342 CRL-3216). All cells were maintained in D10 media (DMEM supplemented with 10% heat-inactivated
343 fetal bovine serum, 2 mM L-glutamine, 100 U of penicillin/ml, and 100 µg of streptomycin/ml) at 37
344 °C at 5 % CO₂.

345 Wildtype A/WSN/1933 (H1N1) influenza virus was generated by reverse genetics using the
346 plasmids pHW181-PB2, pHW182-PB1, pHW183-PA, pHW184-HA, pHW185-NP, pHW186-NA, pHW187-
347 M, and pHW188-NS (*Hoffmann et al., 2000*). The sequences of the viral RNAs encoded in these
348 plasmids are in Figure 1-source data 1. Reverse-genetics plasmids encoding the synonymously
349 barcoded WSN virus were created by using site-directed mutagenesis to introduce two synonymous
350 mutations near the 3' end of the mRNA for each viral gene. The sequences of the synonymously
351 barcoded viral RNAs are in Figure 1-source data 1.

352 To generate viruses from these plasmids, we transfected an equimolar mix of all eight plasmids
353 into cocultures of 293T and MDCK-SIAT1 cells seeded at a ratio of 8:1. At 24 hours post-transfection,
354 we changed media from D10 to influenza growth media (Opti-MEM supplemented with 0.01% heat-
355 inactivated FBS, 0.3% BSA, 100 U of penicillin/ml, 100 µg of streptomycin/ml, and 100 µg of calcium
356 chloride/ml). At 48 hours post-transfection we harvested the virus-containing supernatant, pelleted
357 cellular material by centrifugation at 300 x g's for 4 minutes, and stored aliquots of the clarified
358 viral supernatant at -80 °C. We then titered thawed aliquots of viral by TCID50 on MDCK-SIAT1 cells,
359 computing titers via the formula of *Reed and Muench* (1938). To generate our "high-purity" stocks of
360 viruses for the single-cell sequencing experiments, we then infected MDCK-SIAT1 cells at an MOI of
361 0.01, and let the virus replicate for 36 hours prior to harvesting aliquots that were again clarified by

362 low-speed centrifugation, aliquoted, stored at -80 °C, and titered by TCID50. The high-MOI passage
363 (high-defective particle) stock used in Figure 2 was generated by instead passaging in MDCK-SIAT1
364 cells twice at an MOI of 1 for 48 hours.

365 For the experiments in Figure 7-Figure supplement 1, we created a virus that carried an HA gene
366 segment in which GFP replaced most of the HA coding sequence, following a scheme first described
367 by *Marsh et al. (2007)*. Briefly, we created a plasmid encoding a viral RNA with GFP in place of the
368 HA coding sequence in the context of the pH21 (*Neumann et al., 1999*) reverse-genetics plasmid,
369 removing potential start codons upstream of the GFP (see Figure 7-source data 2 for the sequence
370 of the viral RNA). We then generated GFP-carrying virus by reverse-genetics in cells constitutively
371 expressing HA (*Doud and Bloom, 2016*). To obtain sufficient titers, this HA-eGFP virus was expanded
372 for 44 rather than 36 hours after initiating infection at an MOI of 0.01.

373 qPCR

374 For the qPCR in Figure 2 and Figure 5-Figure supplement 1, A549 cells were seeded at 3x10⁵
375 cells per well in a 6-well tissue culture plate in D10 the day prior to infection. On the day of
376 infection, a single well was trypsinized and the cells were counted in order to determine the
377 appropriate amount of virus to use to achieve the intended MOI. Immediately before infection,
378 D10 was replaced with influenza growth media. For cells incubated with cyclohexamide, the
379 compound was added to a final concentration of 50 µg/ml at the time of infection – previously
380 confirmed to be sufficient to halt viral protein production (*Killip et al., 2014*). RNA was purified
381 using the QIAGEN RNeasy plus mini kit following manufacturer's instructions. cDNA was syn-
382 thetized using an oligoDT primer and the SuperScript™ III first-strand synthesis supermix from
383 ThermoFisher using the manufacturer's protocol. Transcript abundance was measured using
384 SYBR™ green PCR master mix, using a combined anneal/extension step of 60 °C for one minute
385 with the following primers: *HA*: 5'-GGCCCAACCACACATTCAAC-3', 5'-GCTCATCACTGCTAGACGGG-
386 3', *IFNB1*: 5'-AAACTCATGAGCAGTCTGCA-3', 5'-AGGAGATCTTCAGTTCGGAGG-3', *L32*: 5'-
387 AGCTCCCAAAAATAGACGCAC-3', 5'-TTCATAGCAGTAGGCACAAAGG-3'. Biological triplicates were per-
388 formed for all samples.

389 For the measurements of viral genomic HA content in Figure 2A, vRNA was harvested from 80
390 µl of viral supernatant by the addition of 600 µl of RLT plus before proceeding with the standard
391 QIAGEN RNeasy Plus Mini kit protocol. The cDNA was generated using SuperScript™ III first-strand
392 synthesis supermix using the manufacturer's protocol, and using the universal vRNA primers of
393 *Hoffmann et al. (2001)* with the modifications described in *Xue et al. (2017)*. The qPCR was then
394 performed as for mRNA measurements. A standard curve was generated from three independent
395 dilutions of the HA-encoding reverse genetics plasmid. All vRNA values represent three independent
396 RNA extractions with two replicate qPCR measurements.

397 Flow cytometry titering and analyses

398 To determine viral titers in terms of HA-expressing units and for the flow cytometry in Figure 7-
399 Figure supplement 1, A549 cells were seeded in a 6-well plate and infected as described above for
400 the qPCR analyses. Cells were harvested by trypsinization, resuspended in phosphate-buffered
401 saline supplemented with 2% heat-inactivated FBS, and stained with 10 µg/ml of H17-L19, a mouse
402 monoclonal antibody confirmed to bind to WSN HA in a prior study (*Doud et al., 2017*). After
403 washing in PBS plus 2% FBS, the cells were stained with a goat anti-mouse IgG antibody conjugated
404 to APC. Cells were then washed, fixed in 1% formaldehyde, and washed further before a final
405 resuspension and analysis. We then determined the fraction of cells that were HA positive and
406 calculated the HA-expressing units.

407 For Figure 7-Figure supplement 1, after gating to exclude multiplets in FlowJo, data were ex-
408 tracted using the R package flowCore (*Le Meur et al., 2007*) and analyzed using a custom Python
409 script. Guassian kernel density estimates were obtained using the scipy stats package method,
410 gaussian_kde, using automatic bandwidth determination (*van der Walt et al., 2017*).

411 **Infections for single-cell mRNA sequencing**

412 Single-cell sequencing libraries were generated using the 10x Chromium Single Cell 3' plat-
413 form ([Zheng et al., 2017](#)) using the V1 reagents.

414 All time points except for the 8-hour replicate were prepared on the same day. For the infections,
415 A549 cells were seeded in a 6-well plate, with two wells per time point. A single well of cells was
416 trypsinized and counted prior to initiation of the experiment for the purposes of calculating MOI.
417 Wild-type and synonymously barcoded virus were mixed to an estimated ratio of 1:1 based on prior,
418 exploratory, single-cell analyses (data not shown). At the initiation of our experiment, the wells
419 for all time points were changed from D10 to influenza growth media. Cells were then infected
420 with 0.3 HA-expressing units of virus per cell (a determined by flow cytometry). The infections
421 were performed in order of time point: first the 10-hour time point, then the 8-hour, and then the
422 6-hour time point. At one hour after infection, the media for each time point was changed to fresh
423 influenza growth media. Note that the HA-expressing units were calculated without this additional
424 washing step, and so likely represent an overestimate of our final infectious dose (consistent
425 with the fact that fewer than 30% of cells appear infected in the single-cell sequencing data). All
426 cells were then harvested for single-cell analysis concurrently – ensuring all had spent equivalent
427 time in changed media . For our replicate 8-hour time point, cells were infected as above except
428 that the cells were infected at 0.1 HA-expressing units of virus per cell but no wash step was
429 performed, and the sample was prepared on a different day. After harvest, cells were counted using
430 disposable hemocytometers and diluted to equivalent concentrations with an intended capture
431 of 3000 cells/sample following the manufacturer's provided by 10x Genomics for the Chromium
432 Single Cell platform. All subsequent steps through library preparation followed the manufacturer's
433 protocol. Samples were sequenced on an Illumina HiSeq. The deep sequencing data are available
434 on the Sequence Read Archive under accession [[Upload in progress.](#)]

435 **Computational analysis of single-cell mRNA sequencing data**

436 Jupyter notebooks that perform all of the computational analyses are available in Supplemen-
437 tary file 1.

438 Briefly, the raw deep sequencing data were processed using the 10X Genomics software package
439 CellRanger (version 2.0.0). The reads were aligned to a concatenation of the human and influenza
440 virus transcriptomes. The human transcriptome was generated by filtering genome assembly
441 GRCh38 for protein coding genes defined in the GTF file GRCh38.87. The influenza virus transcrip-
442 tome was generated from the reverse-complement of the wildtype WSN viral RNA sequences as
443 encoded in the reverse-genetics plasmids (Figure 1-source data 1). CellRanger calls cells based on
444 the number of observed cell barcodes, and creates a cell-gene matrix. We used custom Python
445 code to annotate the cells in this matrix by the number of viral reads that could be assigned to
446 the wildtype and synonymously barcoded virus. Only about half of the viral reads overlapped
447 the barcoded regions of the genes (Figure 1A) and could therefore be assigned to a viral barcode
448 (Figure 4-Figures supplement 1). So for calculations of the number of reads in a cell derived from
449 each viral barcode for each viral gene, the total number of detected molecules of that gene are
450 multiplied by the fraction of those molecules with assignable barcodes that are assigned to that
451 barcode. This annotated cell-gene matrix is in Supplementary file 2. A Jupyter notebook that
452 performs these analyses is in Supplementary file 1.

453 The annotated cell-gene matrix was analyzed in R, primarily using the Monocle package (version
454 2.4.0) ([Qiu et al., 2017; Trapnell et al., 2014](#)). A Jupyter notebook that performs these analyses is in
455 Supplementary file 1. For each sample, cell barcodes that had >2.5-fold fewer or more UMI counts
456 mapping to cellular transcripts than the sample mean were excluded from downstream analyses
457 (see red vertical lines in Figure 3B).

458 In order to determine an appropriate cutoff for how many reads a cell needed to contain in
459 order to be classified as infected, we calculated the mean viral barcode purity across all cells that
460 contained at least a given fraction of viral mRNA and had multiple viral reads that could be assigned

461 a barcode (Figure 4B,C). We then determined the threshold fraction of viral mRNA at which the mean
462 purity no longer increased as a function of the amount of viral mRNA. This threshold represents
463 the point at which we have effectively eliminated cells that have low barcode purity simply due to
464 lysis-acquired reads sampled randomly from both viral barcodes. The 10-hour sample has the most
465 viral mRNA, and so is expected to have the most lysis-associated influenza reads. We therefore
466 determined the threshold using just this sample, and then applied this threshold to all samples. The
467 threshold is shown in Figure 4C. This procedure is expected to be conservative, and may miss some
468 truly infected cells with very low amounts of viral mRNA. For subsequent analyses, we retained
469 all infected cells and a subsample of uninfected cells (the greater of 50 or the number of infected
470 cells for that sample). The rationale for subsampling the uninfected cell is that the vast majority
471 of cells are uninfected, and we did not want these cells to completely dominate the downstream
472 analyses. Cells were classified as co-infected if both viral variants had an RNA level that exceeded
473 the threshold, and if the minor variant contributed at least 5% of the viral mRNA.

474 For the semi-supervised t-SNE clustering, we used Monocle's cell hierarchy function to bin cells
475 into those with no viral mRNA, <2% viral mRNA, between 2% and 20% viral mRNA, and >20%.
476 Candidate marker genes for t-SNE dimensionality reduction were then determined using the
477 Monocle function markerDiffTable, excluding the effects of sample variation and the number of
478 genes identified in a given cell, using a q-value cutoff of 0.01. The specificity of these markers was
479 determined using the function calculateMarkerSpecificity – the top 40 markers were retained, and
480 used to place populations in a two-dimensional plane based on tSNE dimensionality reduction.

481 For the analyses of cellular genes that differed in expression as a function of the amount of viral
482 mRNA, we only considered cells that expressed all 8 viral mRNAs to avoid effects driven simply by
483 viral gene absence. We also only considered cellular genes in the differential gene analysis, since
484 viral gene expression will tautologically co-vary with the amount of viral mRNA. Additionally, because
485 influenza virus has the capacity to degrade or prevent the synthesis of host mRNAs (*Bercovich-Kinori et al., 2016*) and contributes significantly to the total number UMIs in some cells, we calculate
486 size factors (a scalar value representing efficiency of UMI capture) based on cellular transcripts alone.
487 Finally, we assigned all cells a ceiling fraction of mRNA from virus of 25% so that a few extremely
488 high-expressing cells did not dominate. Cellular genes with expression that co-varied with the
489 fraction of viral mRNAs in a cell were then determined using the Monocle differentialGeneTest, after
490 removing variance explained by sample to sample variation. Figure 9 shows all genes that were
491 significantly associated with the fraction of mRNA from virus at a false discovery rate of 0.1.
492

493 Acknowledgments

494 We thank Xiaojie Qiu for advice about use of the Monocle software package, David Bacsik and Robert
495 Bradley for comments on the manuscript, and the Fred Hutch Genomics Core for performing the
496 Illumina deep sequencing. This work was supported by NIH grant R01GM102198 (to JDB), NIH grant
497 R01AI127893 (to JDB), NIH grant DP2HD088158 (to CT), a Burroughs Wellcome Young Investigator
498 in the Pathogenesis of Infectious Diseases grant (to JDB), and a W. M. Keck Foundation grant
499 (to CT). ABR is supported by a Damon Runyon Fellowship. JDB is partly supported by a Faculty
500 Scholars Award from the Howard Hughes Medical Institute and the Simons Foundation. CT is partly
501 supported by an Alfred P. Sloan Foundation Research Fellowship. The funders had no role in study
502 design, data collection and analysis, decision to publish, or preparation of the manuscript.

503 References

- 504 Aguilera ER, Erickson AK, Jesudhasan PR, Robinson CM, Pfeiffer JK. Plaques formed by mutagenized viral
505 populations have elevated coinfection frequencies. *mBio*. 2017; 8(2):e02020.
- 506 Akpinar F, Timm A, Yin J. High-Throughput Single-Cell Kinetics of Virus Infections in the Presence of Defective
507 Interfering Particles. *Journal of Virology*. 2016 Jan; 90(3):1599–1612.

- 508 Amatore D, Sgarbanti R, Aquilano K, Baldelli S, Limongi D, Civitelli L, Nencioni L, Garaci E, Ciriolo MR, Palamara
509 AT. Influenza virus replication in lung epithelial cells depends on redox-sensitive pathways activated by
510 NOX4-derived ROS. *Cellular microbiology*. 2014 Oct; 17(1):131–145.
- 511 Avraham R, Haseley N, Brown D, Penaranda C, Jijon HB, Trombetta JJ, Satija R, Shalek AK, Xavier RJ, Regev A, et al.
512 Pathogen cell-to-cell variability drives heterogeneity in host immune responses. *Cell*. 2015; 162(6):1309–1321.
- 513 Banning A, Deubel S, Kluth D, Zhou Z, Brigelius-Flohe R. The GI-GPx Gene Is a Target for Nrf2. *Molecular and
514 Cellular Biology*. 2005 May; 25(12):4914–4923.
- 515 Bercovich-Kinori A, Tai J, Gelbart IA, Shitrit A, Ben-Moshe S, Drori Y, Itzkovitz S, Mandelboim M, Stern-Ginossar
516 N. A systematic view on influenza induced host shutoff. *eLife*. 2016 Aug; 5:e18311.
- 517 Bhushal S, Wolfsmüller M, Selvakumar TA, Kemper L, Wirth D, Hornef MW, Hauser H, Köster M. Cell polarization
518 and epigenetic status shape the heterogeneous response to Type III interferons in intestinal epithelial cells.
519 *Frontiers in immunology*. 2017; 8:671.
- 520 Bloom JD. An experimentally determined evolutionary model dramatically improves phylogenetic fit. *Molecular
521 Biology and Evolution*. 2014; 31(8):1956–1978.
- 522 Brooke CB, Ince WL, Wrammert J, Wrammert J, Ahmed R, Wilson PC, Bennink JR, Yewdell JW. Most Influenza A
523 Virions Fail To Express at Least One Essential Viral Protein. *Journal of Virology*. 2013 Feb; 87(6):3155–3162.
- 524 Brooke CB. Biological activities of ‘noninfectious’ influenza A virus particles. *Future Virology*. 2014 Jan; 9(1):41–51.
- 525 Brooke CB, Ince WL, Wei J, Bennink JR, Yewdell JW. Influenza A virus nucleoprotein selectively decreases
526 neuraminidase gene-segment packaging while enhancing viral fitness and transmissibility. *Proceedings of
527 the National Academy of Sciences*. 2014; 111(47):16854–16859.
- 528 Buganim Y, Faddah DA, Cheng AW, Itsikovich E, Markoulaki S, Ganz K, Klemm SL, van Oudenaarden A, Jaenisch R.
529 Single-cell expression analyses during cellular reprogramming reveal an early stochastic and a late hierachic
530 phase. *Cell*. 2012; 150(6):1209–1222.
- 531 Cai L, Friedman N, Xie XS. Stochastic protein expression in individual cells at the single molecule level. *Nature*.
532 2006; 440(7082):358–362.
- 533 Chen S, Chen S, Short JAL, Young DF, Killip MJ, Schneider M, Schneider M, Goodbourn S, Randall RE. Heterocellular
534 induction of interferon by negative-sense RNA viruses. *Virology*. 2010 Nov; 407(2):247–255.
- 535 Chua MA, Schmid S, Perez JT, Langlois RA, et al. Influenza A virus utilizes suboptimal splicing to coordinate the
536 timing of infection. *Cell reports*. 2013; 3(1):23–29.
- 537 Combe M, Garijo R, Geller R, Cuevas JM, Sanjuán R. Single-cell analysis of RNA virus infection identifies multiple
538 genetically diverse viral genomes within single infectious units. *Cell host & microbe*. 2015; 18(4):424–432.
- 539 Crotta S, Davidson S, Mahlakovi T, Desmet CJ, Buckwalter MR, Albert ML, Staeheli P, Wack A. Type I and type III
540 interferons drive redundant amplification loops to induce a transcriptional signature in influenza-infected
541 airway epithelia. *PLoS Pathogens*. 2013; 9(11):e1003773.
- 542 Delbruck M. The burst size distribution in the growth of bacterial viruses (bacteriophages). *Journal of bacteriology*.
543 1945 Aug; 50(2):131–135.
- 544 Dimmock NJ, Dimmock NJ, Easton AJ, Easton AJ. Defective Interfering Influenza Virus RNAs: Time To Reevaluate
545 Their Clinical Potential as Broad-Spectrum Antivirals? *Journal of Virology*. 2014 Apr; 88(10):5217–5227.
- 546 Dou D, Hernández-Neuta I, Wang H, Östbye H, Qian X, Thiele S, Resa-Infante P, Kouassi NM, Sender V, Henrich K,
547 Mellroth P, Henriques-Normark B, Gabriel G, Nilsson M, Daniels R. Analysis of IAV Replication and Co-infection
548 Dynamics by a Versatile RNA Viral Genome Labeling Method. *Cell reports*. 2017 Jul; 20(1):251–263.
- 549 Doud M, Bloom J. Accurate Measurement of the Effects of All Amino-Acid Mutations on Influenza Hemagglutinin.
550 *Viruses*. 2016 Jun; 8(6):155–17.
- 551 Doud MB, Hensley SE, Bloom JD. Complete mapping of viral escape from neutralizing antibodies. *PLoS
552 Pathogens*. 2017 Mar; 13(3):e1006271.
- 553 Doyle V, Virji S, Crompton M. Evidence that cyclophilin-A protects cells against oxidative stress. *The Biochemical
554 journal*. 1999 Jul; 341 (Pt 1)(Pt 1):127–132.

- 555 **Duong HQ**, You K, Oh S, Kwak SJ, Seong YS. Silencing of NRF2 Reduces the Expression of ALDH1A1 and ALDH3A1
556 and Sensitizes to 5-FU in Pancreatic Cancer Cells. *Antioxidants*. 2017 Sep; 6(3):52–10.
- 557 **Eisfeld AJ**, Neumann G, Kawaoka Y. At the centre: influenza A virus ribonucleoproteins. *Nature reviews Microbiology*. 2015; 13(1):28.
- 559 **Elowitz MB**, Levine AJ, Siggia ED, Swain PS. Stochastic gene expression in a single cell. *Science*. 2002;
560 297(5584):1183–1186.
- 561 **Fensterl V**, Sen GC. The ISG56/IFIT1 gene family. *Journal of Interferon & Cytokine Research*. 2011 Jan; 31(1):71–
562 78.
- 563 **Fonville JM**, Marshall N, Tao H, Steel J, Lowen AC. Influenza Virus Reassortment Is Enhanced by Semi-
564 infectious Particles but Can Be Suppressed by Defective Interfering Particles. *PLoS Pathogens*. 2015 Oct;
565 11(10):e1005204.
- 566 **García-Sastre A**, Egorov A, Matassov D, Brandt S, Levy DE, Durbin JE, Palese P, Muster T. Influenza A virus lacking
567 the NS1 gene replicates in interferon-deficient systems. *Virology*. 1998; 252(2):324–330.
- 568 **Geiss GK**, Salvatore M, Tumpey TM, Carter VS, Wang X, Basler CF, Taubenberger JK, Bumgarner RE, Palese
569 P, Katze MG, García-Sastre A. Cellular transcriptional profiling in influenza A virus-infected lung epithelial
570 cells: the role of the nonstructural NS1 protein in the evasion of the host innate defense and its potential
571 contribution to pandemic influenza. *Proceedings of the National Academy of Sciences of the United States of
572 America*. 2002 Aug; 99(16):10736–10741.
- 573 **Gorrini C**, Harris IS, Mak TW. Modulation of oxidative stress as an anticancer strategy. *Nature Publishing Group*.
574 2013 Dec; 12(12):931–947.
- 575 **Hagai T**, Chen X, Miragaia RJ, Gomes T, Rostom R, Kunowska N, Proserpio V, Donati G, Bossini-Castillo L, Naamati
576 G, Emerton G, Trynka G, Kondova I, Denis M, Teichmann SA. Gene expression variability across cells and
577 species shapes innate immunity. *bioRxiv*. 2017; doi: 10.1101/137992.
- 578 **Hale BG**, Randall RE, Ortín J, Jackson D. The multifunctional NS1 protein of influenza A viruses. *Journal of
579 General Virology*. 2008; 89(10):2359–2376.
- 580 **Hatada E**, Hasegawa M, Mukaigawa J, Shimizu K, Fukuda R. Control of influenza virus gene expression: quanti-
581 tative analysis of each viral RNA species in infected cells. *The Journal of Biochemistry*. 1989; 105(4):537–546.
- 582 **Heldt FS**, Frensing T, Reichl U. Modeling the intracellular dynamics of influenza virus replication to understand
583 the control of viral RNA synthesis. *Journal of Virology*. 2012; 86(15):7806–7817.
- 584 **Heldt FS**, Kupke SY, Dorl S, Reichl U, Frensing T. Single-cell analysis and stochastic modelling unveil large
585 cell-to-cell variability in influenza A virus infection. *Nature communications*. 2015 Nov; 6:1–12.
- 586 **Hoffmann E**, Stech J, Guan Y, Webster RG, Perez DR. Universal primer set for the full-length amplification of all
587 influenza A viruses. *Archives of virology*. 2001 Dec; 146(12):2275–2289.
- 588 **Hoffmann E**, Neumann G, Kawaoka Y, Hobom G, Webster RG. A DNA transfection system for generation of
589 influenza A virus from eight plasmids. *Proceedings of the National Academy of Sciences*. 2000; 97(11):6108–
590 6113.
- 591 **Huang AS**, Baltimore D, et al. Defective viral particles and viral disease processes. *Nature*, London. 1970;
592 226:325–7.
- 593 **Huang IC**, Li W, Sui J, Marasco W, Choe H, Farzan M. Influenza A Virus Neuraminidase Limits Viral Superinfection.
594 *Journal of Virology*. 2008 Apr; 82(10):4834–4843.
- 595 **Huang T**, Palese P, Krystal M. Determination of influenza virus proteins required for genome replication. *Journal
596 of Virology*. 1990; 64(11):5669–5673.
- 597 **Hutchinson EC**, von Kirchbach JC, Gog JR, Digard P. Genome packaging in influenza A virus. *Journal of general
598 virology*. 2010; 91(2):313–328.
- 599 **Iwasaki A**, Pillai PS. Innate immunity to influenza virus infection. *Nature Reviews Immunology*. 2014 May;
600 14(5):315–328.
- 601 **Jiang X**, An Z, Lu C, Chen Y, Du E, Qi S, Yang K, Zhang Z, Xu Y. The protective role of Nrf2-Gadd45b against
602 antimony-induced oxidative stress and apoptosis in HEK293 cells. *Toxicology Letters*. 2016 Aug; 256:11–18.

- 603 **Jung KA**, Lee S, Kwak MK. NFE2L2/NRF2 Activity Is Linked to Mitochondria and AMP-Activated Protein Kinase Signaling in Cancers Through miR-181c/Mitochondria-Encoded Cytochrome C Oxidase Regulation. *Antioxidants & Redox Signaling*. 2017 Apr; p. ars.2016.6797-3.
- 606 **Kallfass C**, Lienenklaus S, Weiss S, Staeheli P. Visualizing the beta interferon response in mice during infection with influenza A viruses expressing or lacking nonstructural protein 1. *Journal of Virology*. 2013 Jun; 87(12):6925-6930.
- 609 **Killip MJ**, Jackson D, Perez-Cidoncha M, Fodor E, Randall RE. Single-cell studies of IFN- β promoter activation by wild-type and NS1-defective influenza A viruses. *Journal of General Virology*. 2017 Mar; 98(3):357-363.
- 611 **Killip MJ**, Smith M, Jackson D, Randall RE. Activation of the Interferon Induction Cascade by Influenza A Viruses Requires Viral RNA Synthesis and Nuclear Export. *Journal of Virology*. 2014 Mar; 88(8):3942-3952.
- 613 **Killip MJ**, Fodor E, Randall RE. Influenza virus activation of the interferon system. *Virus research*. 2015 Feb; .
- 614 **Kim KH**, Jeong JY, Surh YJ, Kim KW. Expression of stress-response ATF3 is mediated by Nrf2 in astrocytes. *Nucleic Acids Research*. 2009 Oct; 38(1):48-59.
- 616 **Klein AM**, Mazutis L, Akartuna I, Tallapragada N, Veres A, Li V, Peshkin L, Weitz DA, Kirschner MW. Droplet Barcoding for Single-Cell Transcriptomics Applied to Embryonic Stem Cells. *Cell*. 2015 May; 161(5):1187-1201.
- 618 **Lauring AS**, Andino R. Quasispecies Theory and the Behavior of RNA Viruses. *PLoS Pathogens*. 2010 Jul; 6(7):e1001005-8.
- 620 **Le Meur N**, Hahne F, Ellis B, Haaland P. FlowCore: data structures package for flow cytometry data. Bioconductor Project; 2007.
- 622 **Lee D**, Ryu KY. Effect of cellular ubiquitin levels on the regulation of oxidative stress response and proteasome function via Nrf1. *Biochemical and Biophysical Research Communications*. 2017 Apr; 485(2):234-240.
- 624 **Leonard AS**, Weissman D, Greenbaum B, Ghedin E, Koelle K. Transmission Bottleneck Size Estimation from Pathogen Deep-Sequencing Data, with an Application to Human Influenza A Virus. *Journal of Virology*. 2017; p. JVI-00171-17.
- 627 **Lin X**, Wang R, Zou W, Sun X, Liu X, Zhao L, Wang S, Jin M. The Influenza Virus H5N1 Infection Can Induce ROS Production for Viral Replication and Host Cell Death in A549 Cells Modulated by Human Cu/Zn Superoxide Dismutase (SOD1) Overexpression. *Viruses*. 2016 Jan; 8(1):13-16.
- 630 **Lopez CB**. Defective Viral Genomes: Critical Danger Signals of Viral Infections. *Journal of Virology*. 2014 Jul; 88(16):8720-8723.
- 632 **Van der Maaten L**, Hinton G. Visualizing data using t-SNE. *Journal of Machine Learning Research*. 2008; 9:2579-2605.
- 634 **MacLeod AK**, Acosta-Jimenez L, Coates PJ, McMahon M, Carey FA, Honda T, Henderson CJ, Wolf CR. Aldo-keto reductases are biomarkers of NRF2 activity and are co-ordinately overexpressed in non-small cell lung cancer. *British journal of cancer*. 2016 Dec; 115(12):1530-1539.
- 637 **Macosko EZ**, Basu A, Satija R, Nemesh J, Shekhar K, Goldman M, Tirosh I, Bialas AR, Kamitaki N, Martersteck EM, et al. Highly parallel genome-wide expression profiling of individual cells using nanoliter droplets. *Cell*. 2015; 161(5):1202-1214.
- 640 **von Magnus P**. Incomplete forms of influenza virus. *Advances in Virus Research*. 1954; 2:59-79.
- 641 **Marsh GA**, Hatami R, Palese P. Specific residues of the influenza A virus hemagglutinin viral RNA are important for efficient packaging into budding virions. *Journal of Virology*. 2007; 81(18):9727-9736.
- 643 **McCrone JT**, Woods RJ, Martin ET, Malosh RE, Monto AS, Lauring AS. The evolutionary dynamics of influenza A virus within and between human hosts. *bioRxiv*. 2017; p. 176362.
- 645 **Miura T**, Taketomi A, Nishinaka T, Terada T. Regulation of human carbonyl reductase 1 (CBR1, SDR21C1) gene by transcription factor Nrf2. *Chemico-Biological Interactions*. 2013 Feb; 202(1-3):126-135.
- 647 **Murray J**, Taylor SW, Zhang B, Ghosh SS, Capaldi RA. Oxidative Damage to Mitochondrial Complex I Due to Peroxynitrite. *Journal of Biological Chemistry*. 2003 Sep; 278(39):37223-37230.

- 649 **Neumann G**, Watanabe T, Ito H, Watanabe S, Goto H, Gao P, Hughes M, Perez DR, Donis R, Hoffmann E, Hobom
650 G, Kawaoka Y. Generation of influenza A viruses entirely from cloned cDNAs. *Proceedings of the National
651 Academy of Sciences of the United States of America*. 1999 Aug; 96(16):9345–9350.
- 652 **Nobusawa E**, Sato K. Comparison of the mutation rates of human influenza A and B viruses. *Journal of Virology*.
653 2006; 80(7):3675–3678.
- 654 **Noda T**, Sagara H, Yen A, Takada A, Kida H, Cheng RH, Kawaoka Y. Architecture of ribonucleoprotein complexes
655 in influenza A virus particles. *Nature*. 2006; 439(7075):490.
- 656 **Padovan-Merhar O**, Nair GP, Biaesch A, Mayer A, Scarfone S, Foley SW, Wu AR, Churchman LS, Singh A, Raj
657 A. Single mammalian cells compensate for differences in cellular volume and DNA copy number through
658 independent global transcriptional mechanisms. *Molecular Cell*. 2015; 58(2):339.
- 659 **Parvin JD**, Moscona A, Pan W, Leider J, Palese P. Measurement of the mutation rates of animal viruses: influenza
660 A virus and poliovirus type 1. *Journal of Virology*. 1986; 59(2):377–383.
- 661 **Pauly MD**, Procario MC, Lauring AS. A novel twelve class fluctuation test reveals higher than expected mutation
662 rates for influenza A viruses. *eLife*. 2017; 6:e26437.
- 663 **Perez JT**, Varble A, Sachidanandam R, Zlatev I, Manoharan M, García-Sastre A, et al. Influenza A virus-generated
664 small RNAs regulate the switch from transcription to replication. *Proceedings of the National Academy of
665 Sciences*. 2010; 107(25):11525–11530.
- 666 **Perez-Cidoncha M**, Killip MJ, Oliveros JC, Asensio VJ, Fernandez Y, Bengoechea JA, Randall RE, Ortín J. An
667 Unbiased Genetic Screen Reveals the Polygenic Nature of the Influenza Virus Anti-Interferon Response.
668 *Journal of Virology*. 2014 Apr; 88(9):4632–4646.
- 669 **Peuchant E**, Bats ML, Moranvillier I, Lepoivre M, Guittot J, Wendum D, Lacombe ML, Moreau-Gaudry F, Boissan
670 M, Dabernat S. Metastasis suppressor NM23 limits oxidative stress in mammals by preventing activation of
671 stress-activated protein kinases/JNKs through its nucleoside diphosphate kinase activity. *The FASEB Journal*.
672 2017 Mar; 31(4):1531–1546.
- 673 **Poon LL**, Song T, Rosenfeld R, Lin X, Rogers MB, Zhou B, Sebra R, Halpin RA, Guan Y, Twaddle A, DePasse JV,
674 Stockwell TB, Wentworth DE, Holmes EC, Greenbaum B, Peiris JSM, Cowling BJ, Ghedin E. Quantifying influenza
675 virus diversity and transmission in humans. *Nature Genetics*. 2016; 48(2):195–200.
- 676 **Qiu X**, Mao Q, Tang Y, Wang L, Chawla R, Pliner HA, Trapnell C. Reversed graph embedding resolves complex
677 single-cell trajectories. *Nature Methods*. 2017 Aug; p. 1–10.
- 678 **Raj A**, Peskin CS, Tranchina D, Vargas DY, Tyagi S. Stochastic mRNA synthesis in mammalian cells. *PLoS Biology*.
679 2006; 4(10):e309.
- 680 **Rand U**, Rinas M, Schwerk J, Nöhren G, Linnnes M, Kröger A, Flossdorf M, Kullai KK, Hauser H, Höfer T, Köster M.
681 Multi-layered stochasticity and paracrine signal propagation shape the type-I interferon response. *Molecular
682 Systems Biology*. 2012 Jan; 8(1):584.
- 683 **Reed LJ**, Muench H. A simple method of estimating fifty percent endpoints. *American journal of epidemiology*.
684 1938; 27(3):493–497.
- 685 **Saira K**, Lin X, DePasse JV, Halpin R, Twaddle A, Stockwell T, Angus B, Cozzi-Lepri A, Delfino M, Dugan V, Dwyer
686 DE, Freiberg M, Horban A, Losso M, Lynfield R, Wentworth DN, Holmes EC, Davey R, Wentworth DE, Ghedin E.
687 Sequence analysis of in vivo defective interfering-like RNA of influenza A H1N1 pandemic virus. *Journal of
688 Virology*. 2013; 87(14):8064–8074.
- 689 **Schulte MB**, Andino R. Single-Cell Analysis Uncovers Extensive Biological Noise in Poliovirus Replication. *Journal
690 of Virology*. 2014 May; 88(11):6205–6212.
- 691 **Sgarbanti R**, Amatore D, Celestino I, Marcocci ME, Fraternale A, Ciriolo MR, Magnani M, Saladino R, Garaci E,
692 Palomara AT, Nencioni L. Intracellular redox state as target for anti-influenza therapy: are antioxidants always
693 effective? *Current topics in medicinal chemistry*. 2014; 14(22):2529–2541.
- 694 **Shalek AK**, Satija R, Adiconis X, Gertner RS, Gaublomme JT, Raychowdhury R, Schwartz S, Yosef N, Malboeuf C,
695 Lu D, et al. Single-cell transcriptomics reveals bimodality in expression and splicing in immune cells. *Nature*.
696 2013; 498(7453):236–241.

- 697 **Shalek AK**, Satija R, Shuga J, Trombetta JJ, Gennert D, Lu D, Chen P, Gertner RS, Gaublomme JT, Yosef N, et al.
698 Single cell RNA Seq reveals dynamic paracrine control of cellular variation. *Nature*. 2014; 510(7505):363.
- 699 **Shapiro GI**, Gurney T, Krug RM. Influenza virus gene expression: control mechanisms at early and late times of
700 infection and nuclear-cytoplasmic transport of virus-specific RNAs. *Journal of Virology*. 1987 Mar; 61(3):764-
701 773.
- 702 **Suárez P**, Valcarcel J, Ortín J. Heterogeneity of the mutation rates of influenza A viruses: isolation of mutator
703 mutants. *Journal of Virology*. 1992; 66(4):2491-2494.
- 704 **Suárez-López P**, Ortín J. An estimation of the nucleotide substitution rate at defined positions in the influenza
705 virus haemagglutinin gene. *Journal of general virology*. 1994; 75(2):389-393.
- 706 **Sutejo R**, Yeo DS, Zu Myaing M, Hui C, Xia J, Ko D, Cheung PC, Tan BH, Sugrue RJ. Activation of Type I and III
707 Interferon Signalling Pathways Occurs in Lung Epithelial Cells Infected with Low Pathogenic Avian Influenza
708 Viruses. *PLoS ONE*. 2012; 7(3).
- 709 **Tapia K**, Kim Wk, Sun Y, Mercado-López X, Dunay E, Wise M, Adu M, López CB. Defective viral genomes arising
710 in vivo provide critical danger signals for the triggering of lung antiviral immunity. *PLoS Pathogens*. 2013;
711 9(10):e1003703.
- 712 **Trapnell C**, Cacchiarelli D, Grimsby J, Pokharel P, Li S, Morse M, Lennon NJ, Livak KJ, Mikkelsen TS, Rinn JL. The
713 dynamics and regulators of cell fate decisions are revealed by pseudotemporal ordering of single cells. *Nature
714 Biotechnology*. 2014 Mar; 32(4):381-386.
- 715 **Varble A**, Albrecht RA, Backes S, Crumiller M, Bouvier NM, Sachs D, García-Sastre A, et al. Influenza A virus
716 transmission bottlenecks are defined by infection route and recipient host. *Cell host & microbe*. 2014;
717 16(5):691-700.
- 718 **Vreede FT**, Jung TE, Brownlee GG. Model Suggesting that Replication of Influenza Virus Is Regulated by
719 Stabilization of Replicative Intermediates. *Journal of Virology*. 2004 Aug; 78(17):9568-9572.
- 720 **van der Walt S**, Colbert SC, Varoquaux G. The NumPy Array: A Structure for Efficient Numerical Computation.
721 *Computing in Science & Engineering*. 2017 Aug; 13(2):22-30.
- 722 **Xue J**, Chambers BS, Hensley SE, López CB. Propagation and Characterization of Influenza Virus Stocks That
723 Lack High Levels of Defective Viral Genomes and Hemagglutinin Mutations. *Frontiers in microbiology*. 2016
724 Mar; 7(Pt 10):e1004924-15.
- 725 **Xue KS**, Stevens-Ayers T, Campbell AP, Englund JA, Pergam SA, Boekh M, Bloom JD. Parallel evolution of
726 influenza across multiple spatiotemporal scales. *eLife*. 2017 Jun; 6:e26875.
- 727 **Zheng GX**, Terry JM, Belgrader P, Ryvkin P, Bent ZW, Wilson R, Ziraldo SB, Wheeler TD, McDermott GP, Zhu J, et al.
728 Massively parallel digital transcriptional profiling of single cells. *Nature communications*. 2017; 8:14049.
- 729 **Zhu Y**, Yongky A, Yin J. Growth of an RNA virus in single cells reveals a broad fitness distribution. *Virology*. 2009;
730 385(1):39-46.

Supplementary file 1. Computer code for the analyses. This ZIP file contains a Jupyter notebook that runs CellRanger to align and annotate the reads, and a Jupyter notebook that uses Monocle to analyze the cell-gene matrix. The ZIP file also includes associated custom scripts.

Supplementary file 2. The annotated cell-gene matrix in Matrix Market Format.

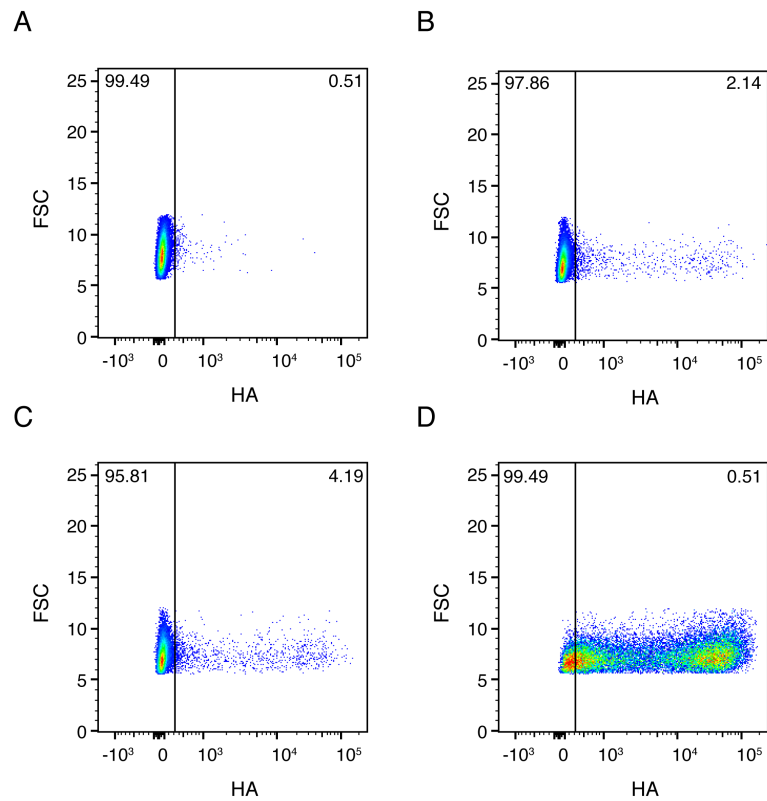


Figure 2-Figure supplement 1. Full flow cytometry date for Figure 2B. A549 cells were infected at an MOI of 0.1 as calculated by TCID₅₀ on MDCK-SIAT1 cells. **(A)** Uninfected gating control. **(B)** Cells infected with the wild-type virus stock used in our experiments. **(C)** Cells infected with synonymously barcoded virus stock used in our experiments. **(D)** Cells infected with a stock of wild-type virus propagated at a high MOI, and therefore enriched in defective particles.

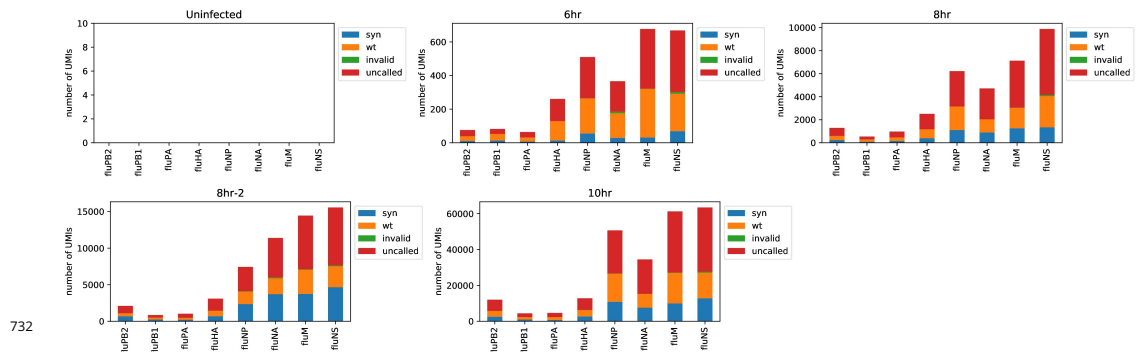


Figure 4-Figure supplement 1. The number of viral barcodes called for each sample and gene segment. Viral transcripts are classified as *syn* if they mapped to a synonymously barcoded influenza transcript, *wt* if they mapped to a wild-type influenza transcript, *invalid* if multiple reads for the same UMI differed on the status of the viral barcode, and as *uncalled* if none of the reads for that UMI overlapped the region of the viral transcript containing the viral barcode. For calculations of the number of reads in a cell derived from each viral barcode for each viral gene, the total number of detected molecules of that gene are multiplied by the fraction of those molecules with assignable barcodes that are assigned to that barcode.

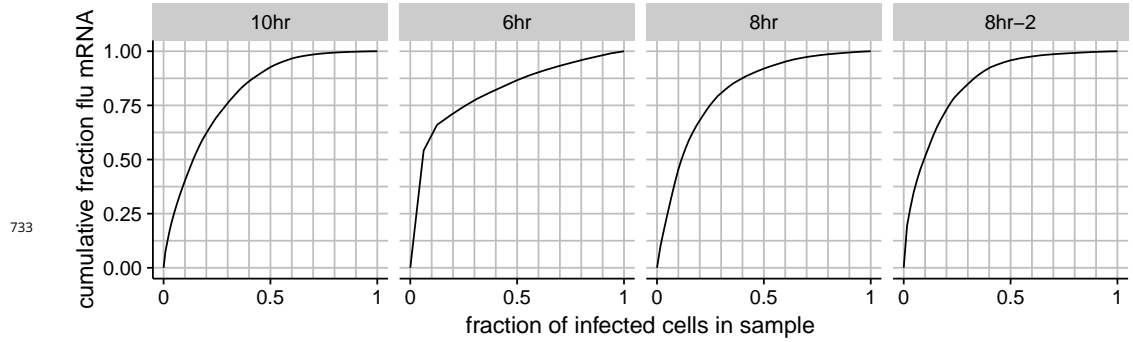


Figure 4–Figure supplement 2. The total fraction of all viral mRNA among infected cells that is attributable to a given fraction of these cells. For instance, the plot for the 8-hour sample shows that roughly 50% of all viral mRNA is derived from 10% of the infected cells.

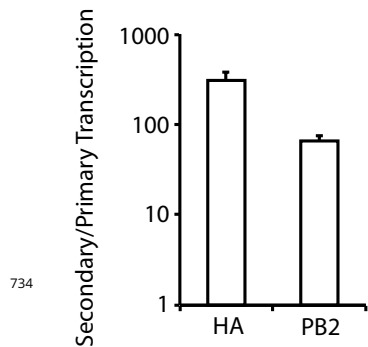


Figure 5–Figure supplement 1. A549 cells were infected at an MOI of 0.2 as calculated on MDCK-SIAT1 cells in either the presence or absence of the protein-translation inhibitor cyclohexamide, and viral mRNA was quantified at 8 hours post-infection by qPCR. The cyclohexamide prevents translation of new PB2, PB1, PA, and NP protein, and so prevents the formation of the new RNP needed for secondary transcription. The bars show the relative amount of HA and PB2 mRNA in the absence versus the presence of cyclohexamide. Error \pm S.D. n=3.

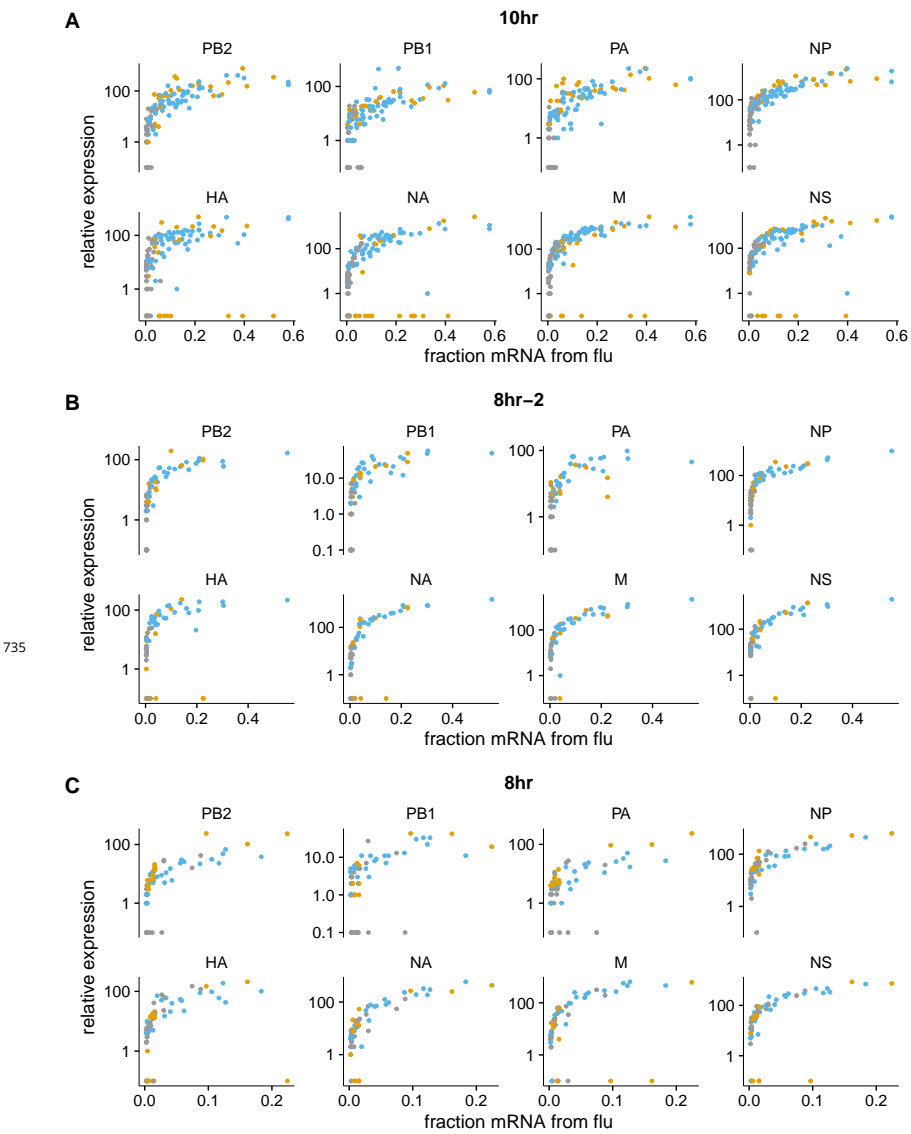


Figure 5–Figure supplement 2. The fraction of mRNA in each infected cell derived as a function of the normalized expression of each viral gene, shown for the 10-hour and 8-hour samples individually (the other samples had too few infected cells for this analysis to be useful). Points are colored as in Figure 5A.

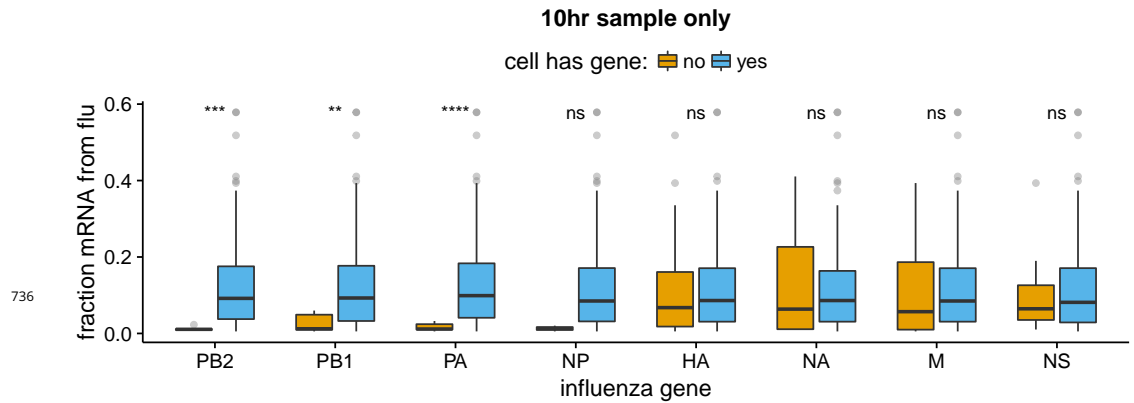


Figure 5–Figure supplement 3. The absence of viral RNP genes but *not* non-RNP genes remains significantly associated with reduced viral burden when we examine only the 10-hr sample, which is the single time point with the most data points. The difference for NP is no longer statistically significant due to low counts of infected cells lacking NP, but the trend remains. We do not show statistical analyses for other samples, as the number of infected cells is too low.

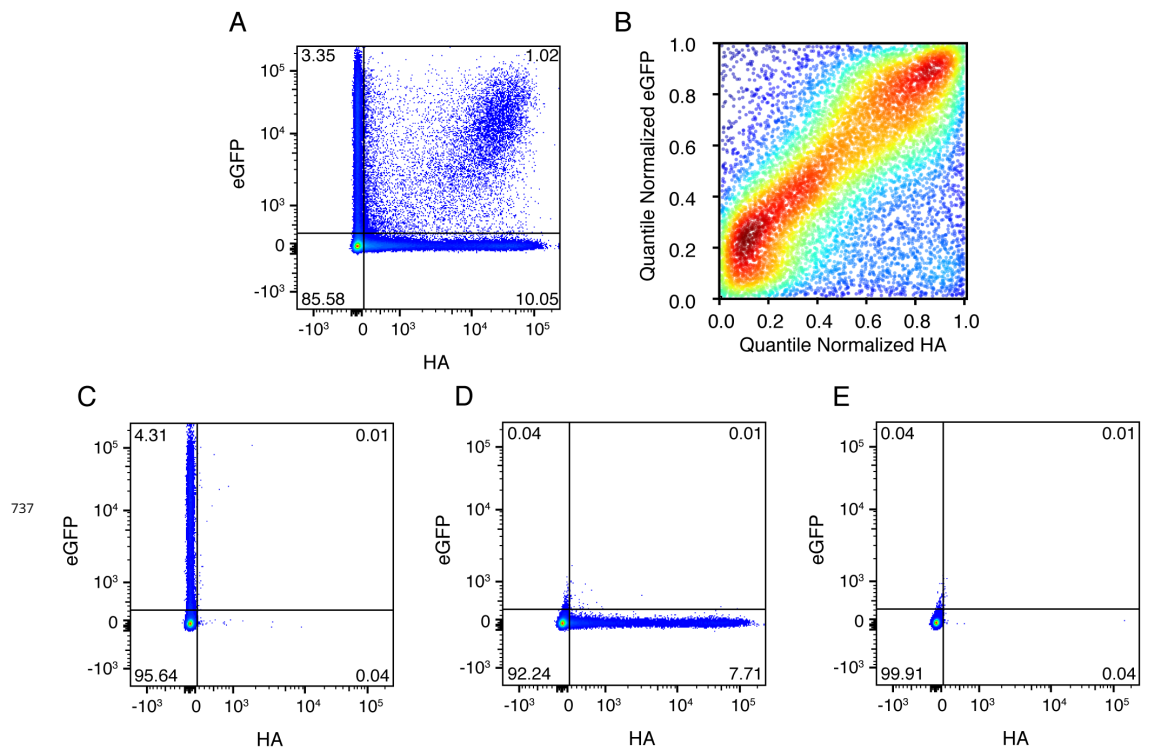


Figure 7–Figure supplement 1. **(A)** Cells were co-infected with a mix of wild-type virus and virus in which the HA gene was replaced by GFP flanked by the terminal regions of the HA gene segment. At 10 hours post-infection, cells were analyzed by flow cytometry for HA and eGFP expression. **(B)** The expression of HA and GFP are correlated in co-infected cells. Shown are the quantile-normalized HA and eGFP signals for double-positive cells. Cells are colored by density, using a Gaussian kernel density estimate. **(C),(D),(E)** Gating controls, single infection with eGFP virus, single infection with wild-type virus, and uninfected cells, respectively.

Category	Genes
Detoxification	AKR1C3, AKR1B10, GPX2, ALDH3A1, ALDH1A1, NQO1, CBR1, PRDX1
Protein folding	TXN, PPIA
Electron transport chain	NDUFB4, MT-CO1, MT-CO3
Regulators	ATF3, GADD45B
ROS-responsive relevance complex/unknown	UBB, NME1

Figure 9–Figure supplement 1. Table delineating genes in Figure 9 that are associated with the response to oxidative stress (*Duong et al., 2017; Jung et al., 2017; Lee and Ryu, 2017; Peuchant et al., 2017; MacLeod et al., 2016; Jiang et al., 2016; Gorrini et al., 2013; Miura et al., 2013; Kim et al., 2009; Banning et al., 2005; Murray et al., 2003; Doyle et al., 1999*).